THE SEA: THE SCIENCE OF OCEAN PREDICTION
Journal of Marine Research, 75, 459–505, 2017

Ocean forecasting for wave energy production

by Alexis Mérigaud[1], Victor Ramos[2], Francesco Paparella, and John V. Ringwood

ABSTRACT

There are a variety of requirements for future forecasts in relation to optimizing the production of wave energy. Daily forecasts are required to plan maintenance activities and allow power producers to accurately bid on wholesale energy markets, hourly forecasts are needed to warn of impending inclement conditions, possibly placing devices in survival mode, while wave-by-wave forecasts are required to optimize the real-time loading of the device so that maximum power is extracted from the waves over all sea conditions. In addition, related hindcasts over a long time scale may be performed to assess the power production capability of a specific wave site. This paper addresses the full spectrum of the aforementioned wave modeling activities, covering the variety of time scales and detailing modeling methods appropriate to the various time scales, and the causal inputs, where appropriate, which drive these models. Some models are based on a physical description of the system, including bathymetry, for example (e.g., in assessing power production capability), while others simply use measured data to form time series models (e.g., in wave-to-wave forecasting). The paper describes each of the wave forecasting problem domains, details appropriate model structures and how those models are parameterized, and also offers a number of case studies to illustrate each modeling methodology.

Keywords: real-time energy markets, time series models, up-wave forecasting, wave forecasting, wave energy resource, wave hindcasting, wave power production assessment, wave spectra

1. Introduction

As the wave energy industry slowly matures, there is a growing need for forecasting of wave conditions, on a variety of time scales, for various activities and needs within the wave energy space. Unlike the case of offshore wind and tidal energy sectors, where the need for sea state forecasting is mainly restricted to installation and maintenance activities, ocean wave prediction is essential for wave energy farms at every stage of project design and planning, commissioning, and operation.

1. Centre for Ocean Energy Research, Maynooth University, Maynooth, Co. Kildare, Ireland
2. Hydraulic Engineering, University of Santiago de Compostela Campus Universitario s/n, 27002, Lugo, Spain

Apart from ocean energy, long- and short-term wave condition forecasts are already useful in a variety of other applications (e.g., navigation, offshore industry, helicopter landing); yet the developing wave industry presents specific needs in terms of wave forecasts, at different time scales, and for a variety of purposes:

(1) In a time scale of several years, assessment of future wave conditions in a given location is essential, for resource assessment, site selection, feasibility studies, and project design. However, for such a long time horizon, no actual meteorological forecast can be reasonably expected. Instead, physical models are used with past input data for at least 10 years, assuming that (1) the past x years are representative of what can be expected in the next x or more years, and (2) the time span considered allows for reasonable coverage of all possible situations. As a consequence, although their purpose is to predict future wave conditions, such studies are specifically referred to as *hindcasts* rather than *forecasts*. A number of hindcast studies have been carried out, and wave hindcasting already presents a reasonable degree of standardization.

In contrast, given the early development stage of the wave energy industry, the use of ocean forecasts *for* and *during* wave farm operation is only slowly emerging, but is equally important:

(2) Daily forecasts are required to plan maintenance activities.
(3) Hourly daily forecasts are required to accurately predict power output from wave farms, allowing farm operators to accurately bid on wholesale energy markets.
(4) Hourly forecasts are required to optimize the operation of wave energy devices, including placing them in a "survival" mode for extreme sea conditions, as necessary.
(5) Wave-by-wave forecasts are required to optimize the computer control that optimizes power capture of wave devices on a wave-by-wave basis.

This paper discusses the needs and tools for wave forecasts from the perspective of the wave energy industry, on three time scales: long-, medium-, and short-term. Long-term forecasts correspond to point (1) above, and thus will more correctly be referred to as hindcasts. Medium-term forecasts cover the application areas of (2) to (4) above, while short-term forecast covers application area (5). The forecasting methods on the three considered time scales differ significantly in terms of approach and use of specific causal inputs.

With a hindcast, the focus is on reconstructing the time history of the sea state in particular specific areas or at particular points within a domain of interest, where, more often, an interpolating numerical wave model (based on physical principles) is driven with wind speed and sea spectrum historical data at the model boundary. The historical boundary input data are themselves typically derived from wider-scale hindcast models (Golding 1983; Group 1988; Tolman 1991; Lo et al. 2008). The process is then equivalent, in the wave energy industry, to wind speed downscaling used for wind turbines within wind farms (Wu and Hong 2007). The physical model of the domain of interest considers local bathymetry, wave generation by wind, and can include other detailed physical processes such as shoaling, refraction, diffraction, reflection, bottom friction, wave breaking, wave–wave interactions

(triad and quadruplet) and wave–current interactions. Such local models are used for a variety of purposes, including detailed resource assessment for sites under consideration for wave energy exploitation. Not only is the mean annual energy resource important, but the variability of the wave condition at different time scales, as well as a detailed, spectral description of the typical wave energy content throughout the year, at the points of interest, is vital to assess the economic value of a wave energy site. As such, the accuracy of hindcasts produced from such models depends to a large extent on the accuracy of the boundary conditions from service providers, as well as the model itself, which is normally calibrated with some specific point measurements from data buoys, for example. It may be noted that the International Electrotechnical Commission (IEC) has recently proposed a series of recommendations to develop a standard methodology for these wide-area models at different levels of resolution.

For medium-term forecasts, the time horizons considered are daily and hourly. The focus is on forecasting the wave condition at a specific point where a wave energy device or farm is operating. In contrast to hindcasts, which already attract significant attention, medium-term forecasts meet needs that will be much more relevant when the wave energy industry has developed to a commercial stage. The more prospective nature of the needs for medium-term wave forecasts justifies some level of discussion. For the time horizons and resolutions considered, a description based on sea states—rather than wave-on-wave—is still relevant. Therefore, physical models of local domains, identical to those used for hindcast, are adequate tools, although the input boundary conditions are not historical data anymore, but wind or sea spectrum forecasts. Alternatively, when the local wave condition can be measured in real time, physical models could possibly be replaced, or complemented, with machine learning and time-series analysis tools.

For short-term wave-on-wave forecasting, a variety of methods can be employed, many of which exploit the strong statistical correlation of the future time series to the recent past. Some methods rely exclusively on past data to estimate either future ocean free-surface elevation at a point, or forecast the *excitation force* experienced by a wave energy device, which is an important quantity in optimizing power capture of a wave energy device. Alternatively, in some cases, free surface elevation forecasts can be determined using up-wave measurements, in tandem with a suitable wave propagation model between the measurement point and the forecast point.

In Section 2, the hindcast methodology and standards are presented. Section 3 discusses in detail the specific needs for medium-term forecasts, and reviews possible techniques, including the physical models presented in Section 2 as well as alternative methods. Finally, Section 4 considers short-term forecasts derived from both autoregressive time series and up-wave measurement approaches.

2. Hindcasting for wave resource characterization

For wave energy to become a commercially viable source of energy, a complete understanding of the wave climate for potential wave energy sites is essential. For this

purpose, data from a network of waveriders or coastal weather stations can supply detailed information at specific locations but, over large areas of seascape, they are not able to provide detailed information about the wave conditions (Gallagher et al. 2016). On the other hand, meteorological agencies run global wind-wave models (Hiles 2010), which use wind velocity estimates to calculate wave development and propagation in off-shore climates (deep oceans), offering a good spatial coverage and providing time-series of offshore wave parameters over long periods of time, allowing for the description of wave climate in locations where measured field data are not available (Camus et al. 2013). Well-known examples of global wind-wave models are the British Met Office Wave Model (BMOWM) (Golding 1983), WaveWatchIII (WW3) (Group 1988), and WAM (Tolman 1991). However, at near-shore locations, the waves computed by these global wind-wave models poorly describe local wave conditions, due to the coarse spatial resolution of global wind-wave models, and the fact that wave transformation processes, caused by the interaction with the bathymetry, are not usually included (Camus et al. 2013). Taking into account these limitations, the state-of-the-art procedure for wave resource assessment is based on: (1) numerical modeling to carry out a downscaling of the meteorological and wave conditions obtained from the global wind-wave models, and (2) model calibration and validation against the wave conditions measured from the waveriders at different coastal locations. Three different downscaling approaches can be found in the literature: (1) a dynamical approach, which consists of nesting, inside a global wind-wave model, a finer wave propagation model to account for the near-shore wave transformation processes such as refraction, bottom friction, shoaling, diffraction and breaking (Iglesias et al. 2000); (2) a statistical approach, which establishes empirical relationships between open-ocean significant wave heights and a nearshore significant wave height in shallow water (i.e., using artificial neural networks [Browne et al. 2007]); and (3) a hybrid approach, which combines dynamical downscaling (numerical models) and statistical downscaling (an interpolation scheme, using neural networks) in order to reduce the computational effort (Herman et al. 2009). Among them, dynamical downscaling seems to be the most accurate approach, since it is able to provide extended time series with a high spatial and temporal resolution, allowing for a better statistical characterization of wave climate and extreme wave analysis (Camus et al. 2013) and, consequently, is the most common approach used for wave resource characterization.

The numerical models most widely used for the dynamical downscaling can be divided into two different categories: phase-averaging wave propagation models and phase-resolving models (Hiles 2010). Phase-averaging wave propagation models or spectral wave models predict the evolution of the surface wave frequency and directional spectrum as waves propagate through varying water depths and ambient currents (Folley et al. 2012). These models are expressed in terms of an energy balance with source and sink terms to represent the different physical processes affecting the wave evolution. Among the main processes influencing wave evolution are wave generation by wind, shoaling, refraction, diffraction, reflection, bottom friction, wave breaking, wave–wave interactions (triad and quadruplet), and wave-current interactions. The main limitation of spectral wave models

is because they do not resolve the propagation of individual waves and, therefore, they are not able to provide information on the phases of the individual waves. This fact renders these models inappropriate to explicitly compute wave diffraction. For this reason, spectral wave models are not suitable for simulating the penetration of waves in complex geometries (harbors) and shallow water applications (van Mierlo 2014).

On the other hand, phase-resolving models deal with the governing equations of the fluid mechanics and are formulated to solve the free surface condition. In addition, phase-resolving models can simulate all wave propagation processes, but not the physics of wave development (wave generation by wind, white-capping, and wave–wave interactions) (Hiles 2010). Phase-resolving models can be subdivided in two different categories: mild-slope and Boussinesq models. The mild-slope models are formulated according to the so-called mild-slope equation, which can be derived from the linear form of Boussinesq shallow water equations. In this case, the vertical dimension of the 3D flow equations is not considered, by assuming that the vertical structure of the flow is equal to the vertical structure of a flow under Airy (linear) waves, and by subsequently integrating over depth (Folley et al. 2012; van Mierlo 2014). Mild-slope models present limitations when it comes to wave amplitude, wave steepness, and bottom slopes, due to the assumption that is made about the vertical structure of the flow. These limitations are equivalent to the limitations of linear or Airy wave theory (van Mierlo 2014). Conversely, the Boussinesq models are based on Boussinesq-type equations that can be derived from potential flow theory, where the vertical dimension from the 3D potential flow equations is also eliminated, but the effects of the vertical structure of the flow are taken into account. The main difference with the mild-slope models is based on the assumption related to the vertical structure of the flow. In this case, the vertical structure is approximated with a perturbation series expansion of the velocity potential at the bottom, instead of assuming the vertical structure of a linear Airy wave (van Mierlo 2014). Finally, the range of application of these kinds of models (mild-slope and Boussinesq) is mainly restricted to assess hydrodynamic behavior under processes related to the propagation of waves from deep to shallow waters and complex bathymetries (e.g., harbors) (Folley et al. 2012; van Mierlo 2014). Furthermore, these models have been applied successfully in wave energy applications such as the estimation of the hydrodynamic interactions and layout optimization of wave energy farms (Folley et al. 2012).

Considering the main characteristics of the different wave models, the spectral wave models (phase-averaging wave propagation models) are the tool most widely used in the literature to carry out wave hindcast for wave resource characterization (Mollison and Pontes 1992; Waters et al. 2009; Liberti et al. 2013). However, the approaches found in the literature vary significantly, especially in terms of the temporal horizons considered for propagation, and the inclusion (or not) of additional aspects such as the seasonal and inter-annual variability of the wave climate, or the effects derived from the wave–current interactions (Vicinanza et al. 2011; Carballo et al. 2014, 2015). In this context, the International Electrotechnical Commission (IEC) has recently proposed a series of recommendations to develop a standard methodology: "*IEC-TS 62600-101: Marine energy –Wave, tidal and other water current*

converters-Part 101: Wave energy resource assessment and characterisation" (from now on referred as IEC-62600-101) (IEC Technical Committee-114 2014), with the aim of ensuring consistency and accuracy in wave resource characterization. For this reason, IEC-62600-101 will be used as a reference in this section in relation to the different aspects of wave resource characterization. Finally, the remainder of this section is structured as follows: Subsection (2a) presents a brief introduction with regard to the theoretical background behind the spectral wave models; Subsection (2b) introduces the main steps for spectral wave modeling setup, and Subsection (2c) presents the main characteristics of wave resource assessment.

a. Spectral wave models

As mentioned in the previous section, spectral wave models are the most suitable kind of models to carry out a dynamic downscaling from a global wind–wave model for wave resource characterization. This subsection presents a brief introduction regarding the main equations solved by the spectral wave models.

i. Wave energy-balance equation. Spectral wave models calculate the development of a sea state based on the wave action density $N(\sigma, \Theta)$, since it is preserved in the presence of ambient currents U, whereas energy density $E(\sigma, \Theta)$ is not (Swan Team 2007). The wave action density is defined as the variance density E divided by the relative frequency (σ), ($N = E/\sigma$). The evolution of the action density is governed by the action balance equation, which can be expressed as:

$$\frac{\partial N}{\partial t} + \nabla \vec{x} \cdot [(\overrightarrow{C_g} + \vec{U})N] + \frac{\partial c_\sigma N}{\partial \sigma} + \frac{\partial c_\theta N}{\partial \theta} = \frac{S_{tot}}{\sigma}. \tag{1}$$

The left side represents the kinematic part of the equation. $\frac{\partial N}{\partial t}$ denotes the evolution of the action density as function of the time. The term $\nabla \vec{x} \cdot [(\overrightarrow{C_g} + \vec{U})N]$ represents the propagation of wave energy with the group velocity $\overrightarrow{c_g} = \partial\sigma/\partial\vec{k}$, following from the dispersion relation $\sigma^2 = g|\vec{k}| \tan h(|\vec{k}|d)$ where $\vec{k}$ is the wave number vector and d the water depth. $\frac{\partial c_\sigma N}{\partial \sigma}$ stands for the effect of shifting the radian frequency due to variations in depth and mean currents. Finally, $\frac{\partial c_\theta N}{\partial \theta}$ represents the effects of the depth and current induced refraction. The quantities c_σ and c_θ stand for the propagation velocities in the spectral space (σ, Θ).

Regarding the right side of Eq. 1, S_{tot} represents the source and sink term, which takes into account the physical processes of generation (S_{in}), dissipation (S_{ds}), and nonlinear wave–wave interactions (S_{nl}):

$$S_{tot} = S_{in} + S_{ds} + S_{nl} \tag{2}$$

ii. Source function terms: Energy input by the wind (S_{in}). The atmosphere has a complex interaction with the wave field. On the one hand, there is a transfer of energy to the wave field by means of the surface stresses exerted by the wind, whereas, on the other hand, the

waves also influence the behavior of the atmospheric layer. Therefore, the wind input term can be written as (Phillips 1957):

$$S_{in}(\sigma, \theta) = A + B \cdot E(\sigma, \theta), \tag{3}$$

where A is the resonant interaction between waves and turbulent pressure patterns (Phillips 1957), while the term $BE(\sigma, \Theta)$ represents the feedback between growing waves and the induced turbulent pressure patterns (Miles 1960).

iii. Source function terms: Energy dissipation (S_{ds}). The three main mechanisms of wave energy dissipation are surf breaking, wave–seabed interaction, and whitecapping. Surf breaking only takes place in extremely shallow waters where water depths and wave heights are of the same order of magnitude (Battjes and Janssen 1978). The wave–seabed dissipation mechanism is mainly due to processes such as bottom friction, percolation, and bottom motions (Shemdin et al. 1978). Finally, whitecapping is the primary mechanism of dissipation in deep water, as during the growth process of the waves, the steepness increases until a point in which the waves break. This process limits the wave growth and is highly nonlinear. Following the World Meteorological Organization (1998), the energy dissipation term can be expressed as

$$S_{ds}(\sigma, \theta) = -\psi(E)\frac{\sigma^2}{\bar{\sigma}}E(\sigma, \theta), \tag{4}$$

where $\psi(E)$ is a property of the integrated energy density spectrum $E(\sigma, \Theta)$, which can be expressed as a function of the wave steepness. Hasselmann et al. (1976) and Komen et al. (1984) developed expressions for $\psi(E)$.

iv. Source function terms: Nonlinear energy transfer by wave–wave interactions (S_{nl}). Nonlinear energy transfer by wave–wave interactions (S_{nl}) represents the propagation of surface waves and the redistribution of energy within the wave spectrum caused by the nonlinear interactions between wave components. In the region of the spectrum close to the peak, the wind input term (S_{in}) is greater than the dissipation (S_{nl}). This excess of energy is redistributed among the higher and lower frequencies. At high frequencies, the energy is dissipated, whereas, at low frequencies, there is a growth of new wave components, resulting in a displacement of the spectral peak toward the lower frequencies. This nonlinear energy transfer was studied by Hasselmann et al. (1976), who found that a group of waves could exchange energy when both the sum of their frequencies and wave numbers was zero. The term S_{nl}, which expresses these energy transfers may be written as follows (World Meteorological Organization 1998):

$$S_{nl}(\sigma, \theta) = f \iiint \delta(k_1 + k_2 - k_3 - k)\delta(\sigma_1 + \sigma_2 - \sigma_3 - \sigma) \times [n_1 n_2 (n_3 + n) - n_3 n(n_1 + n_2)] K dk_1 dk_2 dk_3 \tag{5}$$

where δ is the delta Dirac function, (σ_i, k_i) are the frequency and wavenumber pairs for the interacting wave components, n_i is the wave action density, and K is the Kernel function, which gives the magnitude of the energy transfer to the component k from each combination of interacting waves.

The nonlinear wave–wave interactions (S_{nl}) is by far the most difficult to model, and the different methods used result in a classification of spectral wave models into first, second, and third generation. The first-generation spectral wave models do not present an explicit S_{nl} term; therefore, the nonlinear energy transfers are implicitly expressed in the S_{in} and S_{ds} terms. Regarding the second-generation models, the S_{nl} term is set by parametric methods using, for example, a reference spectrum (JONSWAP; Pierson-Moskowitz) to redistribute the energy over the frequencies. Finally, the third-generation models solve the source term S_{nl} explicitly by the use of special integration methods and the help of numerical approximations (Hasselmann and Hasselmann 1985).

With respect to the accuracy of the different generation wave models, the SWAMP study (1985) (SWAMP Group 1985) proved that the first- and second-generation wave models can be calibrated to obtain reasonable results under a wide range of wind conditions. However, under extreme wind conditions these models are not able to forecast the wave conditions with the required level of accuracy. This fact, alongside the rapid evolution of computing technology, led to the development of the third-generation wave models, which have offered good results in extreme wind and wave conditions (Hasselmann et al. 1976).

v. Wave power per meter of wave front. The components of wave power per meter of wave front (J) are computed from the full wave spectrum according to the following expressions:

$$J_x = \rho g \int_0^{2\pi} \int_0^{\infty} E(\sigma, \theta) C_g(\sigma, d) \cos(\theta) d\sigma d\theta \tag{6}$$

and

$$J_y = \rho g \int_0^{2\pi} \int_0^{\infty} E(\sigma, \theta) C_g(\sigma, d) \sin(\theta) d\sigma d\theta, \tag{7}$$

where J_x and J_y are the wave power components in the x and y directions, respectively; ρ is the water density, g is the acceleration due to gravity, and C_g is the wave group velocity. Therefore, the wave power per meter of wave front, J (Wm^{-1}), is calculated as

$$J = \sqrt{J_x^2 + J_y^2}. \tag{8}$$

b. Spectral wave modeling setup for wave energy resource assessment

In this section, a general introduction for the different aspects related to the implementation of spectral wave model is presented. As mentioned in Section 2, the recommendations

Table 1. Classes of the resource assessments proposed by the IEC-62600-101

Class	Description	Uncertainty	Long-shore extent (km)
Class 1	Reconnaissance	High	>300
Class 2	Feasibility	Medium	20–500
Class 3	Design	Low	<25

IEC, International Electrotechnical Commission (IEC Technical Committee-114 2014).

proposed by the IEC-62600-101 (IEC Technical Committee-114 2014) will be used as a reference. The IEC-62600-101 classifies the resource assessment studies into three different categories: reconnaissance, feasibility, and design, with the notation of Classes 1, 2, and 3, respectively (Table 1). Class 1 is intended to obtain a first approximation of the wave energy resource over a relatively large area of seascape and would be the initial resource assessment conducted in a region. Class 2 assessments are focused on smaller areas that are suitable for refinement of the results obtained from the Class 1 assessments. Finally, Class 3 assessments are used to obtain a detailed characterization in a relatively small area of seascape for the final project design stage, producing results with a low degree of uncertainty. From the modeling standpoint, the effect on the wave model setup process varies considerably depending on the class considered, especially in terms of the boundary condition data and mesh resolution requirements. In addition, IEC-62600-101 also offers a wide set of recommendations regarding the procedure to follow in the fields of data collection, data analysis, and the reporting of the results.

i. Computational domain. Providing the wave model with a suitable computational domain is essential for obtaining reliable results. For this reason, the setup of the computational grids involves the appropriate selection of the area to be modeled, land boundaries, bathymetric resolution, and the characteristic flow and wind fields of the area of study (Benoit 2005.).

In general, two meshing approaches are considered in wave modeling: structured and unstructured grids (Holthuijsen et al. 2000). Structured grids are divided into two different categories: rectilinear and uniform or curvilinear. They always consist of quadrilaterals in which the number of grid cells that meet each other in an internal grid point is 4. The main disadvantage of such a grid is the lack of flexibility to carry out local refinements of the grid, which is a factor of major importance for the simulation of wind waves propagating from deep to shallow waters, where strong bathymetric variations may influence significantly the propagation of the wave conditions. Traditionally, to overcome these problems, a nesting approach is used. The nesting approach is based on computing the wave conditions on a coarse grid for a larger region and then on a finer grid for a smaller region. The computation on the fine grid uses boundary conditions that are generated by the computation on the coarse grid.

On the other hand, unstructured grids may contain triangles or a combination of triangles and quadrilaterals (known as hybrid grids) in which the number of grid cells that meet each

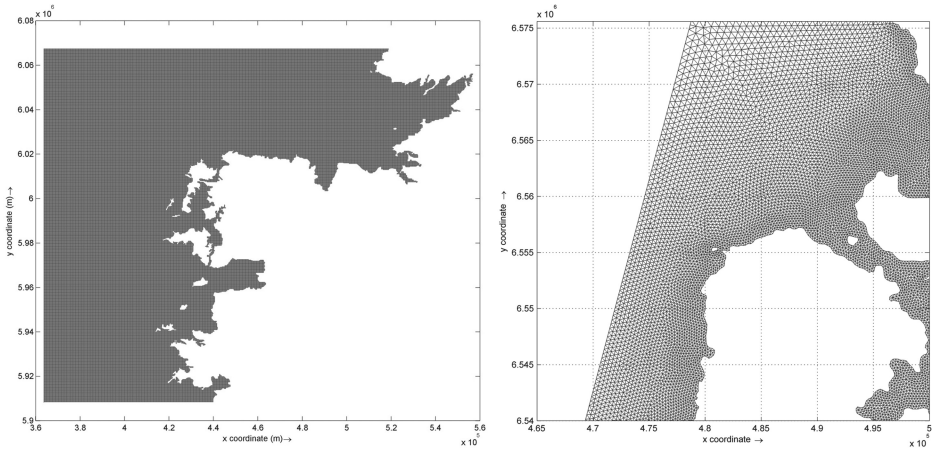

Figure 1. Example of the unstructured grid of a wave model.

other in an internal point of the grid usually ranges from 4 to 10 (Holthuijsen et al. 2000). For this reason, the level of flexibility is far more optimal than the structured grids, which results in much better representation of complex boundaries such as coastlines and areas around islands than do conventional structured grids. In addition, they also provide the opportunity to increase the mesh resolution in the areas of interest (i.e., areas with strong bathymetric variations) to a degree not possible to reach using a structured grid and, therefore, there is no need for nesting. The use of unstructured grids allows the model area to be resolved with a relatively high accuracy, but with much fewer grid points than in the case of structured grids. Finally, although the CPU cost per iteration is higher than cases with structured grids, this fact is more than offset by the reduction in the number of grid points for unstructured grids (Holthuijsen et al. 2000). Figure 1 shows an example of a structured mesh (left) and unstructured mesh (right).

The recommendations of the IEC-62600-101 in terms of grid resolution requirements vary considerably from one class to another. For instance for Class 1 a minimum resolution of 5 km is required, whereas for Classes 2 and 3 the minimum requirements are 500 m and 50 m, respectively.

Finally, in order to account adequately for the propagation of the waves through refraction, shoaling, and bottom friction mechanisms, a bathymetry for the computational model domain has to be prescribed with a sufficient horizontal resolution, especially in shallow waters where the behavior of the waves is strongly influenced by the seabed. According to IEC-62600-101 (IEC Technical Committee-114 2014), the spatial resolution of the bathymetric data should meet the minimum requirements shown in Table 2.

ii. Wave model setup: initial and boundary conditions, physical processes, and numerical settings. To obtain the numerical solution of the action balance (Eq. 1), initial and

Table 2. Resolution of bathymetric data proposed by the IEC-62600-101

Class of assessment	1	2	3
Horizontal resolution in water depths >200 m	5 km	2 km	1 km
Maximum percentage difference in water depth between adjacent bathymetric points in water depths <200 m	10%	5%	2%
Horizontal resolution in water depths <200 m	500 m	100 m	25 m
Horizontal resolution in water depths <20 m	100 m	50 m	10 m

IEC, International Electrotechnical Commission (IEC Technical Committee-114 2014).

wave boundary conditions should be provided. For the initial conditions, it is unusual have measurements that completely characterize the sea state at any one time. Therefore, for numerical wave modeling, the usual course of action is to set to zero the initial elevation above the mean water level and then *spin up* the model with the winds from a certain period (around 10 days [Hasselmann et al. 1976]) prior to the period of interest. This approach is known as a *cold-start* (Hasselmann et al. 1976). On the other hand, the so-called *hot-start* consists of starting the simulation using data from a previous simulation or using available data recorded from field measurement campaigns. However, this latter approach is not totally appropriate, as the wave models generally use a spectral representation of the wave field, which sometimes is difficult to reconstruct from the field measurements. To overcome these deficiencies, several methods are being developed to assimilate wave spectral information derived from radar images (Hasselmann et al. 1976).

With respect to the wave boundary conditions several options are available (IEC Technical Committee-114 2014): (1) parametric boundaries, which are based on a predefined spectral shape (e.g., JONSWAP, Pierson-Moscowitz, Bretschneider) defined by characteristic parameters such as significant wave height, H_{m_0}, peak period, T_p and mean wave direction θ_m, (2) hybrid boundary conditions, characterized by wave spectrum with parametric directional parameters, and (3) spectral boundaries, defined by a directional wave spectrum. Finally, these boundary conditions should be defined using either: (1) physically recorded meteocean data, (2) historical data obtained from a more extensive numerical model (global wind model) or (3) a combination of the first two options.

According to IEC-62600-101, for every class, the boundary condition data should cover a period of at least 10 years (IEC Technical Committee-114. 2014), with a data return rate greater than 70% for the case of the recorded meteocean data, with the aim of obtaining an accurate representation of the wave climate of the region. Furthermore, the IEC-62600-101 also establishes the most appropriate kind of boundary condition for the three classes of resource assessment proposed. Therefore, for Class 3 assessments, spectral boundaries are mandatory and also recommended for the rest of the classes. For Classes 2 and 1, hybrid and parametric boundary conditions are also accepted, respectively.

Finally, regarding the physical processes related to wave propagation such as bottom friction, surf breaking, whitecapping dissipation, nonlinear wave–wave interaction (triads

Table 3. Physical and numeric settings proposed by the IEC-62600-101

Component	Class 1	Class 2	Class 3
Boundary conditions			
Parametric boundary	○	◇	◇
Hybrid boundary	○	○	◇
Spectral boundary	*	*	*
Physical processes			
Wind-wave growth	●	●	●
Whitecapping	●	●	●
Quadruplet interactions	●	●	●
Wave breaking	○	●	●
Bottom friction	○	●	●
Triad interactions	●	●	●
Diffraction	●	●	●
Refraction	●	●	●
Wave reflections	●	●	●
Wave-current interactions	●	●	●
Numerics			
Parametric wave model	○	◇	◇
2nd generation spectral wave model	○	○	◇
3rd generation spectral wave model	*	*	*
Mild-slope wave model	○	○	○
Spherical coordinates	●	○	○
Non-stationary solution	○	○	○
Min. num. wave frequencies	25	25	25
Min. num. azimuthal directions	24	24	24

● Mandatory * Recommended ○ Acceptable ◇ Not permitted IEC, International Electrotechnical Commission (IEC Technical Committee-114 2014).

and quadruplets) should be only considered in the model setup if they are relevant in the area of study. In addition, the adjustment of the formulation parameters of these processes should be carried out against field measurements with the aim of improving the model accuracy. Finally, the main recommendations of IEC-62600-101 for the model setup process of each class are summarized in Table 3.

iii. Model validation. To ensure that the wave model accurately predicts the behavior of the wave propagation, it must be validated against measured wave data. The most common validation parameters for wave modeling are the significant wave height (H_{m0}), energy period (T_e), and omnidirectional wave power (J) (IEC Technical Committee-114 2014; Veigas et al. 2014). In the case of more detailed wave models, additional validation parameters may

Table 4. IEC-62600-101 validation recommendations

Component	Class 1	Class 2	Class 3
Data coverage			
Min. Num. of cell data points	3	5	5
Min. Num. coverage by validation data	90%	90%	95%
Max. acceptable $\boldsymbol{b}(\boldsymbol{e}_p)$			
Sig. wave Height, H_{m_0}	10%	5%	5%
Energy period, *Te*	10%	5%	2%
Omnidirectional wave power, *J*	25%	12%	5%
Dir. of mas dir. resolved power, $\theta_{J\max}$	-	10°	5°
Spectral width, ε_0	-	12%	5%
Directionality coefficient, *d*	-	12%	5%
Max. acceptable $\sigma(\boldsymbol{e}_p)$			
Sig. wave Height, H_{m_0}	15%	10%	7%
Energy period, *Te*	15%	10%	7%
Omni-directional wave power, *J*	35%	25%	20%
Dir. of mas dir. resolved power, $\theta_{J\max}$	-	15°	10°
Spectral width, ε_0	-	25%	15%
Directionality coefficient, *d*	-	25%	15%

be used such as spectral width (ε_0), directionality coefficient (d), and direction of maximum directionally resolved wave power ($\Theta_{J\max}$) (IEC Technical Committee-114 2014; Ramos and Ringwood 2016) . Furthermore, when possible, the model should be validated using data from one or more locations close to the area of interest (i.e., the most energetic regions in the wave resource assessments). Regarding the statistical parameters to assess the accuracy of the model, the most commonly used are the correlation coefficient, R, the root mean square error, *RMSE*, and the scatter index, *SI* (Ramos and Ringwood 2016).

In addition, the IEC-62600-101 proposes a new validation procedure. This new methodology makes a series of recommendations regarding the wave parameters that should be used for validation purposes, the validation periods, the return rate of the recorded data, and the recommended values for the different statistical parameters. The validation data set should cover a period of one year, with a monthly return rate of recorded data exceeding 70%. Then, this data set must be used to construct an omnidirectional $H_{m0}-T_e$ scatter table showing the relative frequency of occurrence of different sea states. Finally, the validation coverage will be defined as the sum of the relative frequency of occurrence of the represented scatter table cells. A cell in the scatter table will be considered to be representative as long as it contains a minimum number of validation data points (Table 4).

The model error is evaluated by considering the data in each scatter table cell, and overall. For each represented cell, the normalized error, *ep*, between measured and modeled values of a parameter, p, must be calculated as

$$e_p = \begin{bmatrix} |(p_{M1} - p_{D1})|/p_{D1} \\ \vdots \\ |(p_{Mn} - p_{Dn})|/p_{Dn} \end{bmatrix}, \tag{9}$$

where p_{Mk} and p_{Dk} are values at coincident time-steps t_k for $k = 1 \ldots n$ of the modeled and measured parameter, respectively. For each cell, the normalized error must be separated into a systematic error, $\mu_{ij}(e_p)$, and a random error, $\sigma_{ij}(e_p)$. The systematic error, or bias, is defined as the mean of errors in cell, (i, j), (Eq. 10), whereas the random error is represented by the standard deviation of the errors in cell, (i, j), (Eq. 11):

$$\mu_{ij} = \frac{1}{N} \sum_{k=1}^{N} e_{p_{ij}} \text{ and} \tag{10}$$

$$\sigma_{ij} = \sqrt{\frac{1}{N-1} \sum_{k=1}^{N} (e_{p_{ij}} - \mu_{ij})^2} \tag{11}$$

The significance of the systematic and random errors at each cell may be related to their influence on the estimation of the energy resource. Therefore, for each cell (i, j), the product of the proportional frequency of occurrence, f_{ij}, and mean incident wave power, J_{ij}, gives a strong indication of any error and should constitute the basis for computing the weighting factor, w_{ij}:

$$w_{ij} = J_{ij} f_{ij} \tag{12}$$

For those cells (i, j), where the minimum number of validation data points is not reached (Table 4), f_{ij}, must be set to zero. Furthermore, if a specific WEC technology is being considered the weighting factor, w_{ij}, may be redefined taking into consideration the capture length, L_{ij}, associated with each cell:

$$w_{ij} = L_{ij} J_{ij} f_{ij}. \tag{13}$$

In any case, the weighting matrix shall be normalized such that its sum is equal to one:

$$w_{ij} = \frac{w_{ij}}{\sum_{i,j} w_{ij}}. \tag{14}$$

Therefore, the weighted mean random error, $\sigma(e_p)$, and the weighted systematic error, $b(e_p)$, can be calculated as the sum of the element-wise product of the normalized weighting matrix and the random and systematic error matrices, respectively:

$$\sigma(e_p) = \sum_{i,j} w_{ij}\, \sigma_{ij} \quad \text{and} \tag{15}$$

$$b(e_p) = \sum_{i,j} w_{ij}\, \mu_{ij}. \tag{16}$$

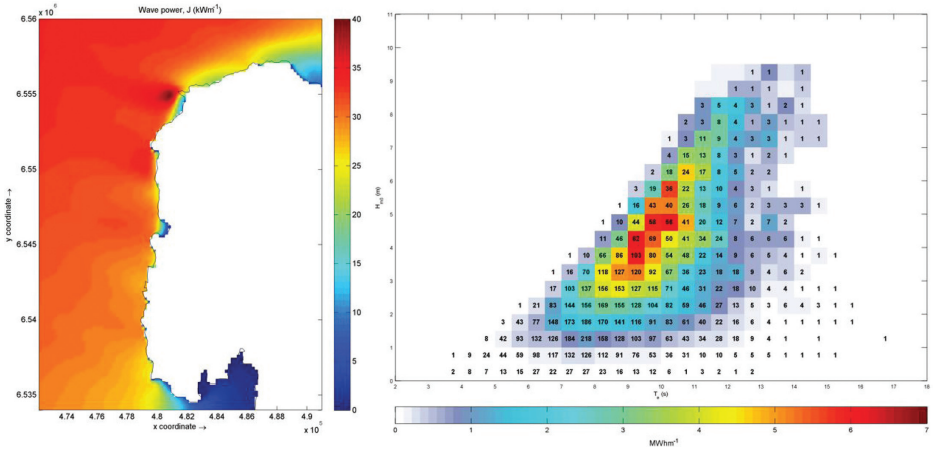

Figure 2. Left: Spatial distribution of wave power over a coastal area. Right: Example of an annual scatter table for a specific location.

Table 4 summarizes, for each class of resource assessment, the maximum acceptable weighted mean systematic and random errors for every validation parameter. This methodology was investigated in detail in (Ramos and Ringwood 2016), proving to be a robust methodology that covers a wide range of wave parameters to assess the accuracy of the model.

c. Wave energy resource characterization

As mentioned in Section 2a, the wave model computes the full spectrum at each grid node, which allows for computing the wave energy power per meter of wave front according to Eq. 6 and Eq. 7 for each wave sea state. Therefore, the spatial distribution for a certain location can be obtained for a period of interest. Figure 2 (left) shows the spatial distribution of wave power over a coastal region calculated from a spectral wave model.

The wave energy resource in a certain location is determined by constructing an omnidirectional scatter table showing the available annual energy and the annual number of h of each sea state, parameterized in terms of H_{m0} and T_e. The scatter tables are essential in understanding how the energy of the waves is distributed among the different sea states, and it also provides a first estimation for the design of the range of operation of wave energy converter (WEC) in a certain location. In addition, the omnidirectional scatter table can also be constructed for shorter temporal horizons (i.e., seasonal, monthly) to assess in detail the seasonality of the wave resource (Carballo et al. 2014, 2015). In addition, directionally resolved annual scatter tables can be constructed, when the wave direction can be relevant for the performance of specific types of WECs.

In both cases, to cover the temporal variability of the wave resource, IEC-62600-101 establishes that, independently of the class considered, the numerical model used to estimate the wave resource should produce a minimum of 10 years of sea state data, which shall be generated with a minimum frequency of one data set every 3 h. For the construction of both the omnidirectional and directionally resolved scatter tables, the dimensions of each bin must be set with a resolution of 0.5 m and 1.0 s of H_{m0} and T_e, with their upper and lower bounds ensuring that a minimum of 99% of sea states are included. Furthermore, in the case of the directionally resolved scatter tables, the maximum directional window shall be 45°, with the sea states partitioned into directional windows based on the direction of maximum directionally resolved wave power (IEC Technical Committee-114 2014). Figure 2 (right) shows an example of an annual scatter table for a specific location over the coastal area shown in the Figure 2 (left).

3. Medium-term forecasts

Medium-term forecasting of ocean meteorological conditions is already required in various sectors such as navigation, offshore oil and gas industry, and ocean energy, in order to plan construction, maintenance, navigation, or other offshore activities, so as to meet safety criteria for the material and personnel involved. From the point of view of construction and maintenance planning, the need for ocean meteorological forecasts, in the field of wave energy, would not present any significant difference, compared to equivalent needs in other existing offshore activities. But when it comes to the wave energy farm operation, other needs arise, which are more specific to the wave energy sector.

First, many wave energy device concepts are featured with a safe mode that, in case of strong seas exceeding some threshold condition, enables them to stop producing power, and to enter a configuration where they are protected from dangerous hydrodynamic loads. Thus, forecasting sea state will not only be necessary when on-site operations are required, but also on an everyday basis to ensure the safe operation of wave energy devices. The threshold condition for entering safe mode can be based, for example, on the significant wave height H_{m_0} of the forecast spectrum (see, for example, (Maisondieu 2015)).

Second, participation of wave energy production in electricity markets will require accurate forecasts of expected power output. Compared to maintenance planning or device survivability, power production forecasts require a more detailed description of the local sea wave spectrum, because the output of wave energy devices, depending on their operating principle, can be sensitive to a variety of parameters such as wave height, wave period, wave direction and spectral bandwidth. The issue of the accuracy of the sea wave spectrum description is discussed in Section 3b.

Among the three main application areas of medium-term forecasting for wave energy, namely maintenance, safe device operation, and market participation, the latter is clearly the most demanding in terms of time resolution and accuracy of the sea state description. It can be assumed that, if it is possible to successfully forecast detailed enough wave

conditions for power output forecasting, then using the same tools for maintenance and safe device operation presents no difficulty. Therefore, in the following, the focus will be more specifically on medium-term wave forecasts for market participation, i.e., wave energy forecasting.

Finally, it should be noted that for any of the purposes detailed here, although forecasts at the longest possible time horizon would always be desirable, reasonably accurate forecasts are only achievable up to 2–3 days ahead, mainly due to the reliance on meteorological inputs.

a. Time horizons and resolutions for wave energy forecasting

Renewable electricity forecasts are becoming more and more essential, both for the power system as a whole, and from the point of view of individual renewable energy producers.

The increasing penetration of intermittent, often decentralized, renewable electricity production makes it more and more difficult for transmission and distribution system operators to ensure the balance of the electrical grid in real time. Additional power capacities, called reserves, are required to be able to face any unforeseen event such as power plant outage, or a renewable electricity production lower than expected. In order to face the intermittency and unpredictability of most nonconventional renewable energy sources (especially wind, solar and wave power), additional means of flexibility have to be integrated into electrical systems, such as gas power plants, energy storage, or demand-side management. Improving the accuracy of renewable energy forecasts would result in limiting the need for additional flexibility and reserve capacity, and then reduce the overall cost of running the electrical network (e.g., see, for the German case, Hirth and Ziegenhagen (2015)).

From the point of view of individual plant operators participating in energy markets, production forecasts are also essential. Electricity trading more than two days ahead is generally handled on a bilateral basis. Then, on medium- to short-term time horizons, electricity is traded on wholesale SPOT markets, which consist of a day-ahead market and, more and more often, an intra-day market that closes up to 30 min before the delivery time. SPOT markets enable market players to balance their positions, taking into account their current trading position, the market price evolution, updates of demand and variable RE forecasts, as well as their production constraints. In parallel to financial transactions on electricity markets, plant operators plan their production in order to honor their sales on electricity markets, and to meet the consumption of their final customers if they are also suppliers. The relevant time horizons for participation in organized SPOT electricity markets are shown in Figure 3.

After intra-day market gate closure, the balance of the entire electrical system is ensured in real time by the transmission system operator (TSO), or by an equivalent organization, through various mechanisms (Wang et al. 2015). Through an *a posteriori* imbalance settlement (Fig. 3), market participants are penalized for the positive or negative difference between their market positions and actual energy deliveries. Therefore, the actual individual energy imbalance of each market participant is computed *ex-post* for each

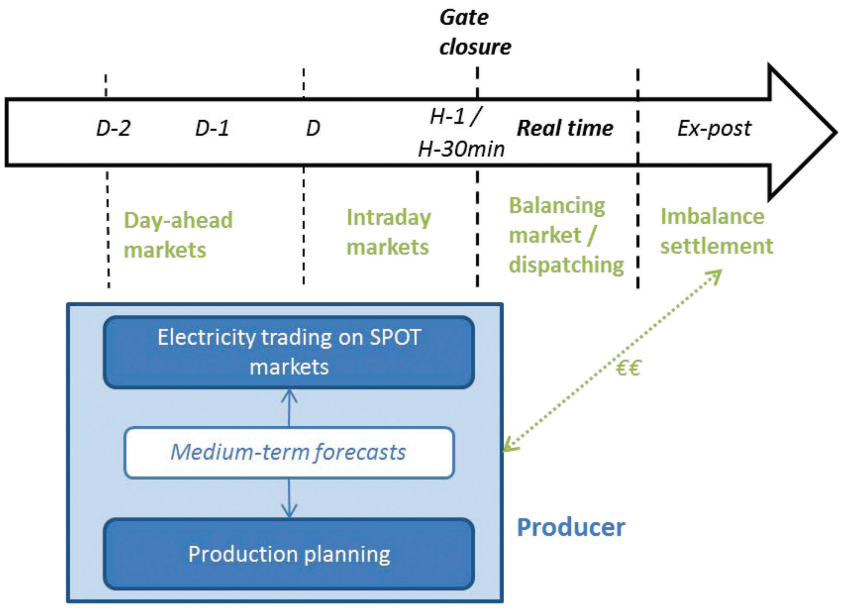

Figure 3. Main time horizons of organized electricity markets.

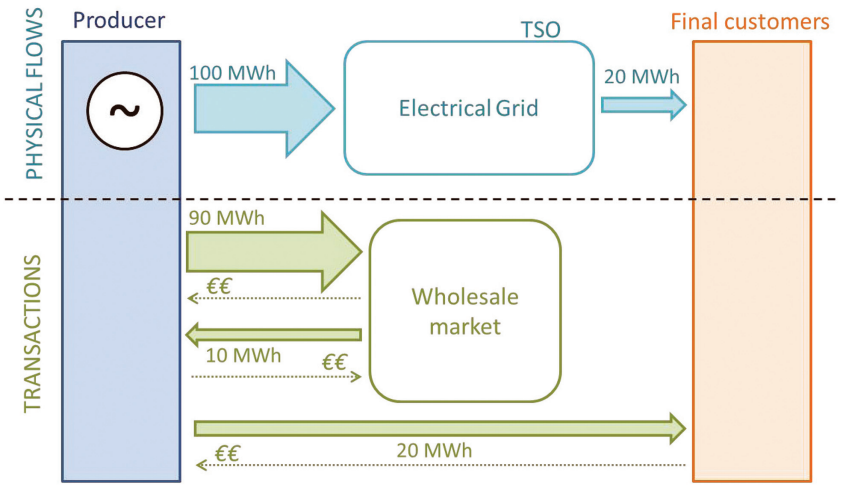

Figure 4. Simplified example of physical and financial flows for an electricity producer.

settlement period: the sum of estimated consumer withdrawals and market sales, on the one hand, is compared with measured production and market purchases, on the other hand, as exemplified in Figure 4. Market participants are penalized for any observed imbalance: a market participant whose imbalance is negative will have to pay for the energy that it failed

to deliver to the system. Conversely, a market participant whose imbalance is positive will be paid for the unplanned, extra amount of energy that it has delivered to the system, but at an unfavorable price. Although the exact penalty system may vary significantly depending on the jurisdiction, the imbalance settlement system is generally designed so that producers, traders, and suppliers are always incentivized to balance their positions ahead of real time, i.e., on SPOT markets. Figure 4 compares, for a given settlement period, the physical and financial flows related to a power producer, who sells the main part of its production on wholesale markets, but also sells a small part of its production through contracts with final customers directly. On this example, purchasing 10 MWh on the SPOT market is necessary for the producer to be in a balanced position – and the unbalance is $100 + 10 - 90 - 20 = 0$ MWh.

It is then clear that forecasts are essential for electricity producers, in order to participate in energy markets while minimizing their imbalance in each imbalance settlement period. Additionally, it seems that:

- Relevant time horizons for production forecasts should coincide with market lead times, i.e., all time horizons between 2–3 days ahead, and 60 or even 30 min ahead (EPEX Spot 2015).
- The imbalance settlement period sets a target value that should be considered as a time step to establish forecast production curves. In practice, the imbalance settlement period is often 1 h (e.g. under the jurisdiction of some North-American independent system operators, such as PJM, ISO-NE, and NYISO), 30 min (e.g., in France), or even shorter, at 15 min (e.g., Germany and Austria) or 10 min (e.g., CAISO, the Californian independent system operator). Thirty minutes is the target set by the current European grid code on Electricity Balancing; however, the Agency for the Cooperation of Energy Regulators (ACER) is pushing forward a 15-min imbalance settlement period before 2019.

Renewable energy is being gradually integrated into power grids through various schemes (for national policies in European countries see, for example, RES Legal Europe (2014)). In some support policy designs for renewable electricity (e.g., in France, Ireland, or Germany), renewable electricity producers are not responsible for directly selling their production on electricity markets, or don't have to pay for their imbalances (Wang et al. 2015). The degree of responsibility of renewable energy producers in balancing can also be mitigated by more flexible balancing settlement rules such as in the US (Aparicio et al. 2012). However, this situation is changing in many jurisdictions in order to allow for integration of renewable energy on an equal footing with conventional power sources. Thus, there is more and more incentive, for renewable electricity producers, to sell their production directly on electricity markets, and to minimize their imbalance themselves, by updating their forecasts and balancing their position on SPOT markets accordingly: this is already the case in Germany for big wind energy producers, and in the UK (Aparicio et al. 2012).

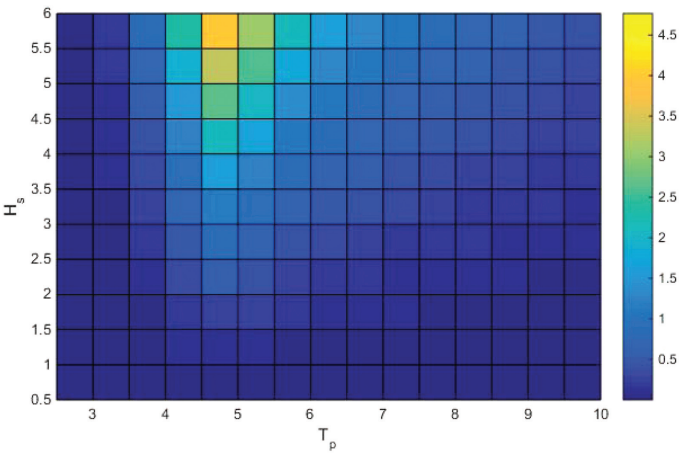

Figure 5. Example of WEC (wave energy converter) power matrix (units in kW).

In summary, the incentive for renewable energy producers to forecast their own production will be increasingly strong, and if wave energy is to be one day developed at an industrial scale, wave energy producers will likely be subject to the same obligations. Therefore, considering the time resolutions and time horizons of electricity markets provides a relevant framework to determine wave energy forecasting requirements. The wave power forecast time horizon should then range at least from two to three days ahead to 1 h ahead (which also coincides with the feasibility range of accurate local meteorological forecasts). The forecasts should consist of a value for energy production every 30 min, which corresponds to an average case for the imbalance settlement period.

b. Wave spectrum characterization for wave energy forecasting

Now that target time horizons and resolutions for medium-term wave forecasting have been defined, it is necessary to determine the level of information that the forecast spectrum should contain, in order to ensure accurate estimates of the WEC or wave farm power output.

i. The power matrix approach. In most studies dedicated to wave resource and WEC performance assessment (see for example De Andres et al. (2013, 2015); Babarit et al. (2012); Babarit (2015), and Section 2), the WECs are described by means of a two-parameter power matrix, whose entries are typically a representative wave period (usually the peak wave period T_p or the mean energy wave period T_e) and the significant wave height H_{m_0} of the spectrum. The power matrix specifies, for each (H_{m_0}, T_p) pair, the expected WEC output. An example power matrix is shown in Figure 5. The power matrix facilitates a very fast computation of the annual power output through convolution with the site scatter

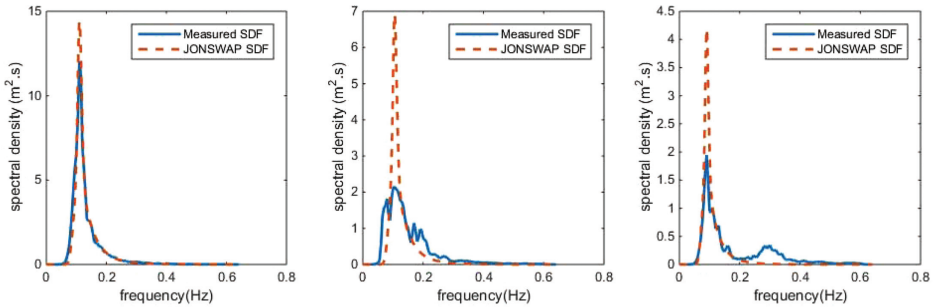

Figure 6. Three examples of half-hourly spectral density functions (SDF) recorded in Belmullet, Ireland, shown with the JONSWAP SDFs having the same H_{m_0} and T_p ($\gamma = 3.3$).

diagram such as described in Section 2. The underlying assumptions behind the power matrix representation are that:

- The wave spectra at the device location can be described accurately in a parametric way, with only two parameters;
- The two spectral parameters are sufficient to characterize the WEC output.

Concerning the first assumption, and depending on the area under study, a unimodal, omnidirectional, two-parameter spectrum is usually considered, such as the JONSWAP or Bretschneider (1959) spectral formulations (for the JONSWAP formulation, the parameter γ is usually assumed to be 3.3). Such an approach focuses on the low-frequency content of the spectrum, and cannot describe multimodal wave spectra combining one or more swells wind seas. Therefore, an actual sea spectrum can significantly differ from a two-parameter spectrum with the same (H_{m_0}, T_p) pair, as illustrated in Figure 6. Additionally, in many locations, the sea condition is multimodal during a significant part of the year. For example, at the three locations studied in De Andres et al. (2015), namely North-West Denmark, North Spain, Chile, and West Ireland, unimodal sea states only represent from 45% to 60% of the total sea states recorded throughout the year. Finally, the directional spread of wave energy cannot be described in an omnidirectional spectrum formulation.

Some WECs could certainly be insensitive to wave directionality and to the high-frequency content of the input wave spectrum, in which case a sea state characterization through an omnidirectional, two-parameter JONSWAP or Bretschneider, spectrum may be sufficient to predict the WEC output. But, in a wide variety of cases, WECs are sensitive to the wave direction and to the energy distribution across wave frequencies. Therefore, describing sea states as a simple (H_{m_0}, T_e) pair may lead to significant over- or underestimation of the WEC power output. De Andres et al. (2015) showed that, for some of the wave energy converters studied, the error made on the power output, for a given spectrum describing a 3-h sea state, could amount to as much as 200% of the true power production.

Within the scope of resource assessment and project design studies, the errors made on individual wave spectra may be averaged out when considering annual power production. However, even over such a long time scale, results presented in De Andres et al. (2015) tend to show that significant error, in the order of 5%–20% of the true average annual power, may remain for some WEC types and geographical locations. The problem of power output estimation error is, of course, much more significant within the scope of medium-term forecasts for wave energy forecasting, since forecast errors are penalized for every time slot considered and thus no averaging of the error is to be expected.

In addition, the level of sophistication of current physical ocean models now makes it possible to describe local wave conditions much more precisely than via just two parameters. In state-of-the-art models, such as in Gallagher et al. (2016), sea states are described as discretized, full-directional spectra, with a spectral resolution of 30 frequencies and 24 directions, and without assuming any predefined spectral shape or combination of spectral shapes. Therefore, it can be reasonably expected that a comprehensive characterization of local wave spectra, for the purposes of forecast and hindcast, can be achieved.

Nevertheless, it may be unrealistic to obtain the WEC power output for every forecast spectrum by means of time-domain simulations at each forecast update. Therefore, some concise, parametric description of sea states are still desirable, in order to easily derive the WEC power output through an improved, possibly multidimensional, version of the power matrix.

ii. Improved spectral descriptions. A rather comprehensive approach would consist of describing the wave spectrum as the sum of a finite number of wave systems (Kerbiriou et al. 2007), each one being described through a standard spectral shape with two or three parameters, e.g., H_{m_0}, T_e and mean wave direction. Such an approach allows for a fairly accurate and physically meaningful description of any wave spectrum. But the number of possible parameter combinations of the multidimensional power matrix increases exponentially with the number of parameters, so that it may be computationally prohibitive to fill in the multidimensional power matrix by means of experiments or numerical simulations. Furthermore, many combinations of parameters are unlikely to be ever encountered in some locations.

Therefore, we focus on more concise sea state descriptions, suggesting only one or two more parameters in addition to H_{m_0} and T_p (Saulnier et al. 2011; Pascal et al. 2012). For WECs or WEC arrays that exhibit a strong sensitivity to the incident wave direction, the average direction of the main wave system may be a relevant additional parameter. Other suggested additional spectral parameters generally provide information about:

- The wave spectrum directional spread (Pascal et al. 2012); and/or
- The wave spectrum frequency spread (or spectral bandwidth) (Saulnier et al. 2011; Pascal et al. 2012).

However, for the WECs tank-tested in Pascal et al. (2012), the directional spread only has a very minor impact on the WEC performance. Concerning the energy spread of the

wave spectrum across frequencies, it is suggested both in Saulnier et al. (2011) and in Pascal et al. (2012) to use an additional parameter related to the spectral bandwidth of the spectrum. Indeed, spectral bandwidth has a strong influence on wave groups (i.e., groups of successive waves exceeding a given threshold), which, in turn, may strongly influence power production. Many different parameters exist that measure the spectral bandwidth (Ochi 2005; Saulnier et al. 2011). For example, in Saulnier et al. (2011), the spectral broadness ε_0, defined as

$$\varepsilon_0 = \sqrt{\frac{m_0 m_{-2}}{m_{-1}^2} - 1}$$

is found to be a useful parameter that does not over-represent high frequencies. In general, the most appropriate spectral bandwidth parameter seems to depend on the WEC model considered.

Bandwidth parameters are particularly suitable for WECs with a broadband response (Saulnier et al. 2011), but may not be sufficient for any WEC and sea state, since even a triplet of values (wave height, wave period, spectral bandwidth) may still be the same for a range of significantly different sea states. In De Andrés et al. (2015), although, in the range of sea states studied, the WEC performance for a fixed (H_{m_0}, T_e) pair roughly follows a linear trend with respect to ε_0, it can also be seen that even with the same $(H_{m_0}, T_e, \varepsilon_0)$ triplet, significantly different power values can be obtained.

An interesting formulation is suggested in Mackay (2016), where, for a given (H_{m_0}, T_e) pair, the spectral shape is characterized by two additional parameters, both taking continuous values between 0 and 1, and governing

- the degree of bimodality;
- the degree of prevalence of swell over wind sea.

Both parameters are directly computed from the omnidirectional spectrum, without resorting to any spectral partitioning method. The total number of parameters then remains relatively modest, and yet may allow for accurate assessment of WEC power output.

Given all of the above, it is clear that medium-term wave forecasts for wave energy conversion will not consist of predicting only one or two spectral parameters. However, in view of the current literature and development of the wave energy industry, it is still difficult to ascertain what exact wave spectrum description will have to be forecast. Most probably, the answer will depend, to a greater or lesser extent, on the WEC type and geographical location under study.

c. Methods for local wave condition forecasting

i. Physical wave models with forecast boundary conditions. The bulk of Section 2 has focused on the calculation of the wave resource on a spatial domain, where boundary conditions of the domain are independently specified. Such models are commonly used for

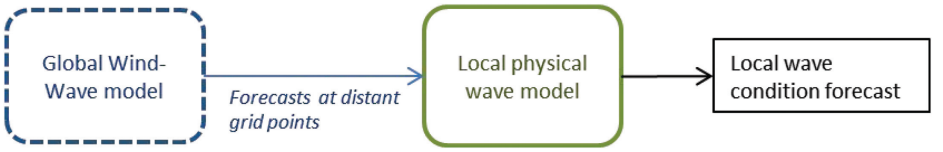

Figure 7. Physical downscaling for medium-term wave forecasts.

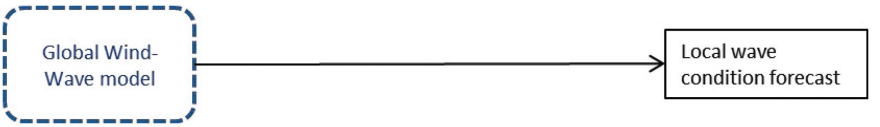

Figure 8. Medium-term wave forecasts through direct use of a global wind-wave model.

hindcasting, where historical measurements of the boundary conditions are available, in order to examine the viability of various specific points within the domain for harnessing wave energy. However, when the effort in building the spatial models on a domain has been completed, these models can then also be used for forecasting the wave conditions at specific points within the constructed domain (Reikard et al. 2015), as indicated in Figure 7.

The only difference is in the input wind and wave boundary conditions, which must consist of forecast data instead of hindcast data. Future values of the boundary conditions can be obtained from meteorological service providers. For example, the European Centre for Medium-Range Weather Forecasts (ECMWF; ECMWF 2017), which is an independent intergovernmental organization, makes its wind and wave condition forecast products freely available. However, it should be ensured that the level of detail, time horizons, and time resolution of the forecast boundary conditions are compatible with those discussed in Sections 3a and 3b. In particular, the time resolution would be significantly more refined: 30 min, compared to the 3 h specified by IEC-62600-101. Such a change would make the physical downscaling models more computationally intensive; however, since the total time duration considered would not exceed 2–3 days, the computational burden would still be compatible with medium-term forecasts.

Finally, let us note that, in some cases, the wave condition forecasts at a location may be directly available from a global wind-wave model, and thus may not require any downscaling (Reikard et al. 2011) (Fig. 8).

The advantages of using physical models to forecast local wave conditions include:

- A sea state description with a comprehensive level of detail can be readily obtained;
- The whole local area can be treated at once, which is useful when one or several WEC farms in the same local area are considered;
- Uncertainty in the forecast can be assessed, especially when forecast boundary conditions are provided as ensemble forecasts.

Figure 9. Non-physical downscaling for medium-term wave forecasts.

The drawbacks of physical models are:

- their computational cost, which can be a significant disadvantage, where frequent and rapid forecast updates must be carried out;
- their complex set up and calibration; and
- their limitation in predicting the short-term evolution of the wave condition, i.e., less than 3 to 6 h ahead, as highlighted in Reikard et al. (2011).

ii. Other methods: Time-series and machine-learning. In view of the aforementioned limitations of physical models, other tools, originating from time-series analysis and machine learning, have been suggested by several authors to replace or complement physical models. A few distinct configurations may be identified:

(1) Downscaling through machine learning

As already pointed out in Section 2, some authors suggest that predicting local wave condition from distant wave conditions, given by global wind–wave models, can be achieved by means of statistical methods instead of a dynamic, physical approach (Fig. 9). For example, in Fernández et al. (2015), machine-learning models are proposed to predict nearshore significant wave height and wave energy flux. In Castro et al. (2014), artificial neural networks (ANN) are compared to a SWAN numerical wave model to predict the nearshore wave power, taking as inputs the significant wave height, mean energy wave period, and mean wave direction at the domain boundaries. In the specific case considered, the ANN model shows comparable performance with respect to the numerical wave model, and can even predict better extreme wave conditions. Studies (Castro et al. 2014; Fernández et al. 2015) deal with downscaling rather than with forecasts *per se*; thus, it should be kept in mind that adapting such statistical methods to the process of forecasting would involve training the models taking boundary condition forecast values as inputs.

The main drawback of statistical downscaling methods is that they necessitate a significant dataset to "learn" the statistical relationship between distant and local wave conditions. Such datasets imply either that there are historical buoy measurements available for the exact location considered, or that a physical model has already been built in order to generate a training dataset. Furthermore, unlike physical wave models that can compute the wave condition at any desired grid point within the local area considered, statistical models can only provide forecasts at one specific point of the local area where the model has been

Figure 10. Time-series analysis for medium-term wave forecasts.

previously trained, and the forecast consists of scalar values (e.g., significant wave height, mean energy wave period, wave energy flux).

(2) Time-series methods

Methods originating from time-series analysis, and already used in a wide range of forecast application areas, can be equally relevant to wave power forecasting, using past measured values to predict the next wave condition, as illustrated in Figure 10. Examples can be found in Reikard et al. (2011, 2015) and Jeon and Taylor (2016), where the methods considered can be based on regression, statistical methods (Reikard et al. 2015; Jeon and Taylor 2016), or on machine learning, e.g., ANNs (Reikard et al. 2011; Hatalis et al. 2014). It was found in comparative studies, such as Reikard et al. (2011), that methods based on time-series analysis are more performant than numerical physical models for the shortest time horizons, i.e., from 1 to 6 h ahead.

The study by Jeon and Taylor (2016) is particularly interesting, since it proposes *density* forecasting, as opposed to *point* forecasting. Such additional probabilistic information can be very useful in applications with a strong variability of the output. The time horizons considered range from 1 to 24 h. Past and present wind and wave values recorded at an offshore meteorological station are used as inputs for the models. Amongst the methods compared, bivariate ARMA-GARCH is found to be a suitable type of model to forecast joint probabilities for pairs of values such as significant wave height and peak wave period. Compared to a direct forecast of the wave energy flux, it seems to be more accurate to forecast wave height and period, and then derive the wave energy flux.

Such methods would require that the wave condition is measured in real-time in the vicinity of the WECs, or that the WECs themselves are able to measure and transmit some information on the sea state in which they are operating.

(3) Hybrid methods

As mentioned earlier, physics-based methods generally perform better for longer time horizons (typically beyond 6 h), while methods based on time-series perform better for short time horizons (below 6 h). Hence, the idea of combining the strong points of both approaches in a hybrid framework has been proposed by some authors, for example in (Reikard et al. 2011; Pinson et al. 2012), as illustrated in Figure 11.

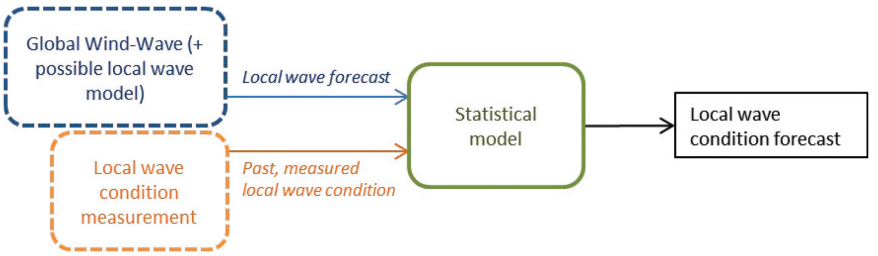

Figure 11. Hybrid method for medium-term wave forecasts.

In Reikard et al. (2011), the hourly significant wave height, mean energy wave period and wave energy flux are predicted at time horizons ranging from 1 h to 48 h, which is suitable in view of the requirements specified in 3.1. Three methods are compared:

- Forecasts from a global wind–wave model;
- Two time-series methods: a simple linear regression and a neural network (nonlinear regression), where past values are taken as inputs to predict future values;
- A hybrid method, in which both the global wind–wave forecasts and the past measured values of sea-state parameters are used as inputs for a regression.

The hybrid method is found to outperform both the purely physical model and the time-series-based methods, regardless of the time horizon considered. The algorithm in Pinson et al. (2012) is based on the method developed in Reikard et al. (2011), but this time probabilistic forecasting is proposed to take into account the uncertainties in the global wind–wave forecasts.

4. Short-term wave forecasting

In contrast to the preceding section, short-term wave forecasting relates to a very specific point in the ocean and focuses on a time scale of seconds, usually up to a maximum time horizon of about a minute. The main purpose of short-term wave forecasting is the optimization of wave energy device operation, while some other applications also exist, for example the prediction of *quiescent periods* in free surface elevation in order to optimize the timing of landing of helicopters on sea vessels.

The energy conversion in most wave energy converters (WECs) is based either on relative oscillation between bodies or on oscillating pressure distributions within fixed or moving chambers. Typically, WECs are designed to have a pronounced resonance over a range of frequencies, where most of the wave energy is available (Falcão 2010). However, in order to cope with variations in the sea state, a control system is designed to alter the dynamics of the device, and realize an efficient absorption of energy for a wider range of frequencies (Korde 2000). In the early development stages, WEC control was based on relationships in the frequency domain, which aimed to maximize the absorbed energy at

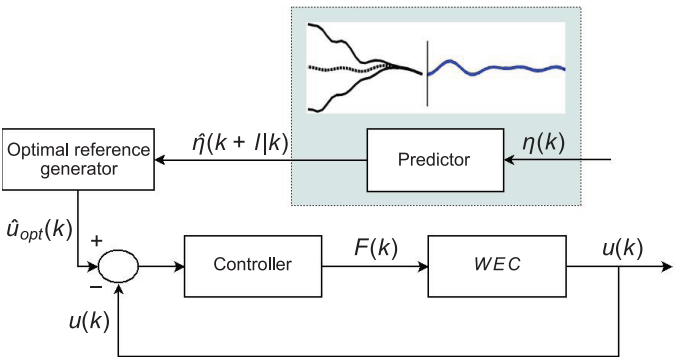

Figure 12. Wave predictions are required in order to generate an optimal reference for a generic time-domain control of a wave energy converter.

each frequency of the incident wave (Korde 2000; Falnes (in press)) . In order to realize the *real-time control* of a WEC, appropriate transformations are required in order to transform the aforementioned frequency relationships into a control law in the time domain. However, such transformations involve noncausal transfer functions that require future knowledge of the motion of the device, or of the wave elevation, in order to realize the optimal energy absorption from the WEC (Korde 2000; Falnes (in press)).

Therefore, forecasting of the incident wave profile at a specific point is fundamental for the more general problem of real-time control of the WEC. As an example, Figure 12 illustrates a possible digital control scheme for a generic oscillating body, where the controlled variable is its oscillation velocity, $u(k)$, and the control action is performed through a control force $F(k)$. Usually, prediction of the wave elevation is based on a spatial reconstruction of the wave field starting from a set of sensors located in the proximity of the WEC, as shown in Figure 13b (Fusco and Ringwood 2010). Another possible solution is to predict the wave elevation based only on its past history, as shown in Figure 13a. Regarding the spatial approach, the forecasting model requires an array of spatial measurements and can become very complex, since it has to take into account the possible multidirectionality of waves (Belmont et al. 2006), the presence of radiated and diffracted waves (Frigaard and Brorsen 1995), and eventual waves propagation nonlinearities (Fusco 2009). Phase-resolving models introduced in Section 2 accurately calculate diffraction, shoaling, refractions, and nonlinearity (Adytia et al. 2012). However, the complexity of phase-resolving models makes them unsuitable for real-time applications.

A number of short-term wave forecasting approaches are possible. In Tedd and Frigaard (2007), digital filters were deployed for the real time prediction of waves incident upon a wave energy device. In Dannenberg et al. (2010), the remote wave profile is measured by means of a nautical radar, and is propagated in time and space in order to predict the spatial wave field profiles and estimate the motion of a vessel. In Belmont et al. (2007),

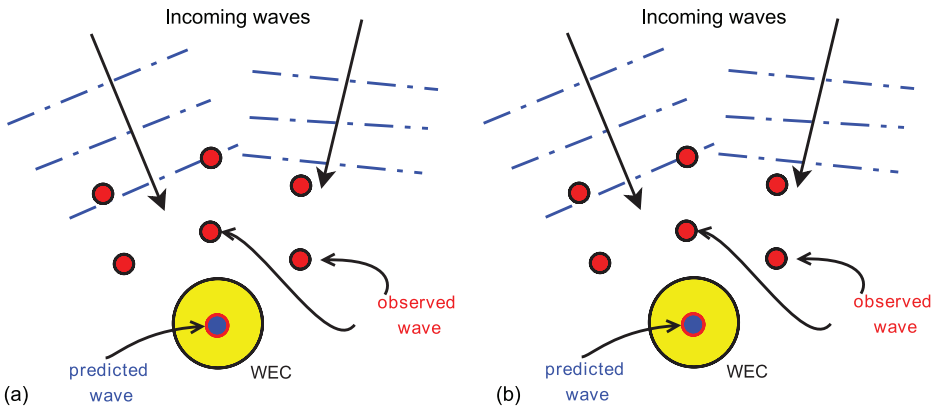

Figure 13. Wave prediction based on one-single point of measurements (a), and wave prediction based on spatial reconstruction from array of sensors (b).

a shallow-angle LIDAR was used to measure the time evolution of sea waves over an extended region of several hundred meters. In Halliday et al. (2011), the Fast Fourier Transform is employed to decompose the wave elevation into individual frequencies at a given point, propagate each individual frequency component using the dispersion relation, and reconstruct the wave elevation at a different temporal and spatial point.

The time series approach for wave prediction has significant advantages over spatial prediction, in terms of complexity of the models (multidirectionality and radiation do not need to be considered unless the WECs device itself is directional) and the amount of instrumentation required (measurements at only one point are required). In Fusco and Ringwood (2010), autoregressive (AR) models are proposed and validated against real observations. In Fischer et al. (2012) adaptive filters based on autoregressive models for wave prediction are deployed. In Schoen et al. (2011), a robust control for wave energy devices based on the prediction of the wave elevation is implemented. For wave prediction, a hybrid Kautz/AR predictive model and a purely predictive Kautz model are proposed. In Price et al. (2007), artificial neural networks for the estimation of the wave excitation force were trained and results compared to other methods.

a. Time-series forecasting

In this section, a variety forecasting models based on the past history of the wave elevation at a given point are presented and validated against real observations (Fusco and Ringwood 2010).

i. Cyclical methods. The most straightforward forecasting model is a cyclical model, where the wave elevation, $\eta(k)$, is expressed as a superposition of a number m of linear harmonic components:

$$\eta(k) = \sum_{i=1}^{m} \alpha_i \cos(\omega_i k) + \beta_i \sin(\omega_i k) + \zeta(k). \tag{19}$$

To estimate the parameters of the model in Eq. 19, the frequencies are kept constant and the model becomes perfectly linear in the parameters α_i, β_i. The choice of frequencies is a crucial one. In Fusco and Ringwood (2009), it was pointed out how, while the range of frequencies is easy to determine, the distribution of the ω_i inside this range is more problematic. A robust choice would be a constant spacing over the complete frequency range, with the spacing as small as possible in order to give an accurate coverage of the spectrum (appropriate constant frequency intervals are also discussed in Nolan et al. 2007). Once the frequencies are determined, a model for the amplitude variations has to be chosen. Initially, the cyclical structural model proposed by Harvey (1989) was adopted:

$$\eta(k) = \sum_{i=1}^{m} \psi_i(k) + \zeta(k) \tag{20}$$

and

$$\begin{bmatrix} \psi_i(k+1) \\ \psi_i^*(k+1) \end{bmatrix} = \begin{bmatrix} \cos(\omega_i T_s) & \sin(\omega_i T_s) \\ -\sin(\omega_i T_s) & \cos(\omega_i T_s) \end{bmatrix} \begin{bmatrix} \psi_i(k) \\ \psi_i^*(k) \end{bmatrix} + \begin{bmatrix} w_i(k) \\ w_i^*(k) \end{bmatrix}, \quad i = 1, \ldots m, \tag{21}$$

where T_s is the sampling time, vectors $[\psi_i(k)\ \psi_i*(k)]^T$ model the m cyclical components, and it can be verified that $\psi_i(0) = \alpha_i$ and $\psi_i^*(0) = \beta_i$. The Gaussian white disturbance $[w_i(k)\ w_i*(k)]^T$ models the amplitude and phases variation. From Eq. 20 and Eq. 21, the following state space form is derived:

$$\begin{aligned} \boldsymbol{x}(k+1) &= \boldsymbol{A}\boldsymbol{x}(k) + \boldsymbol{w}(k) \\ \eta(k) &= \boldsymbol{C}\boldsymbol{x}(k) + \zeta(k), \end{aligned} \tag{22}$$

where

$$\boldsymbol{x}(k) = \left[\psi_1(k)\ \psi_1^*(k) \ldots \psi_m(k)\ \psi_m^*(k)\right]^T \in R^{2m\times 1}, \tag{23}$$

$$\boldsymbol{w}(k) = \left[w_1(k)\ w_1^*(k) \ldots w_m(k)\ w_m^*(k)\right]^T \in R^{2m\times 1}, \tag{24}$$

$$\boldsymbol{A} = \operatorname{diag}\left\{ \begin{bmatrix} \cos(\omega_i T_s) & \sin(\omega_i T_s) \\ -\sin(\omega_i T_s) & \cos(\omega_i T_s) \end{bmatrix} \right\} \in R^{2m\times 2m}, \text{ and} \tag{25}$$

$$\boldsymbol{C} = \begin{bmatrix} 1 & 0 & 1 & 0 \ldots 1 & 0 \end{bmatrix} \in R^{1\times 2m}. \tag{26}$$

The state space form is suited to the application of the Kalman filter for recursive on-line adaption. When the estimate of the model's parameters, $\hat{\boldsymbol{x}}(k|k)$, is available at any instant k, the l-step-ahead prediction $\hat{\eta}(k+l|k)$ is obtained through the free evolution of the model in Eq. 22 as:

$$\hat{\eta}(k+l|k) = \boldsymbol{C}\boldsymbol{A}^l\hat{\boldsymbol{x}}(k|k). \tag{27}$$

ii. Sinusoidal extrapolation with the extended Kalman filter. A step further from the cyclical models with fixed frequencies would be to consider variable frequencies that are updated on-line, along with the amplitudes and phases, on the basis of the free surface wave elevation measurements. We can, therefore, attempt to model the wave elevation as a single cyclical component of the type in Eq. 21, but with a time-varying frequency $\omega(k)$:

$$\eta(k) = \psi(k) + \zeta(k) \tag{28}$$

with

$$\begin{bmatrix} \psi_i(k+1) \\ \psi_i^*(k+1) \\ \omega(k+1) \end{bmatrix} = \begin{bmatrix} \cos(\omega(k)T_s) & \sin(\omega(k)T_s) & 0 \\ -\sin(\omega(k)T_s) & \cos(\omega(k)T_s) & 0 \\ 0 & 0 & 1 \end{bmatrix} \begin{bmatrix} \psi_i(k) \\ \psi_i^*(k) \\ \omega(k) \end{bmatrix} + \begin{bmatrix} \varepsilon(k) \\ \varepsilon^*(k) \\ \kappa(k) \end{bmatrix}, \tag{29}$$

where $\varepsilon(k)$, $\varepsilon^*(k)$, and $\zeta(k)$ are random disturbances, $\eta(k)$ is the wave elevation, and a model for the variability of $\omega(k)$ has been introduced, assuming a simple random walk driven by the additional white noise $\kappa(k)$. The model in Eq. 29 is, of course, nonlinear in $\omega(k)$ and an explicit linear state space structure cannot be formulated. As a consequence, a linear recursive estimator cannot be directly applied. It is possible, however, to utilize an extension of the Kalman filter to nonlinear models, namely the Extended Kalman Filter (EKF), assuming that the discrete time step, T_s, is suffciently small to permit the prediction equations to be approximated by a linearized form, based on the truncation of the Taylor expansion of Eq. 29 at the first order (Quine et al. 1995). The estimate of the state vector at each time step is, therefore, given by linear recursive equations, while the prediction $\hat{\eta}(k+l|k) = \hat{\psi}(k+l|k)$ is obtained from the free evolution of the nonlinear model in Eq. 29.

iii. AR models. The wave elevation $\eta(k)$ is assumed to be linearly dependent on a number, n, of its past values, through the parameters a_i:

$$\eta(k) = \sum_{i=1}^{n} a_i \eta(k-i) + \zeta(k), \tag{30}$$

where a disturbance (or error) term $\zeta(k)$ has been included. If an estimate of the parameters at instant k, i.e., $\hat{a}i(k)$, is computed and the noise $\zeta(k)$ is assumed to be Gaussian and white, the best prediction of the future wave elevation $\hat{\eta}(k+l|k)$ at instant k can be derived from Eq. 30 as:

$$\hat{\eta}(k+l|k) = \sum_{i=1}^{n} \hat{a}_i \eta(k+l-i|k), \tag{31}$$

where, obviously, $\hat{\eta}(k+l-i|k) \equiv \eta(k)$ if $k+l-i \leq k$ (i.e., information already acquired, no need of prediction). The AR coefficients, a_i, are estimated from N batch observations

through the minimization of a multi-step-ahead cost functional, referred to as long-range predictive identification (LPRI) (Shook et al. 1991):

$$J_{LPRI} = \sum_{k=1}^{N} \sum_{j=1}^{N_l} \left[\eta(k) - \hat{\eta}(k|k-j)\right]^2, \tag{32}$$

where N_l is the forecasting horizon over which the AR model is to be optimized. The function J_{LPRI} is minimized with a standard algorithm for nonlinear least squares problems, the Gauss–Newton algorithm, initialized with the estimates from regular least squares (Shook et al. 1991).

iv. Artificial neural networks. In spite of the nonlinear modeling capability, neural networks have the great disadvantage of offering a model completely enclosed in a black box, where inherent characteristics cannot be analyzed by inspection or analytical calculation. So, whereas in the cyclical and AR models an analysis of the estimated parameters and frequencies and their variations in an adaptive structure can provide indications about the real process behavior and its main characteristics, this would not be possible with artificial neural networks. For the problem under study, a nonlinear relationship between past and present wave elevation values is created through a multilayer perceptron (Norgaard et al. 2000):

$$\eta(k) = NN(\eta(k-1), \eta(k-2), \ldots \eta(k-n)). \tag{33}$$

Only structures with 1 linear output neuron and 2 hidden layers, consisting of a number of nonlinear neurons, varying between 3 and 7 each, were considered. Several orders of regression n were also considered. The model is trained using the Levenberg–Marquard algorithm (Wilamowski et al. 2001) on a set of batch data and utilized for multi-step-ahead prediction.

b. Time-series forecasting sample results

To test the forecasting models described in Section 4a, the wave elevation at two locations was recorded (Fusco and Ringwood 2010): (i) the Irish Marine Institute provided real observations from a data buoy located in Galway Bay, on the West Coast of Ireland and (ii) wave elevation time series are also available from the Atlantic Ocean at the Pico Island, in the Azores Archipelago.

The climate at the Galway bay site is dominated by relatively low energy sea states (significant wave height less than 2 m) which, most of the time, has a broad spectral distribution with no clear energy peak, due to the superposition of low frequency swell (s) and high-frequency wind waves of similar energy content. Wave systems off the coast of Pico, on the other hand, usually have a more defined low frequency peak (around 0.7 rad/s) and their significant wave height ranges, usually, from 1 m to 5 m. The wave spectra of three

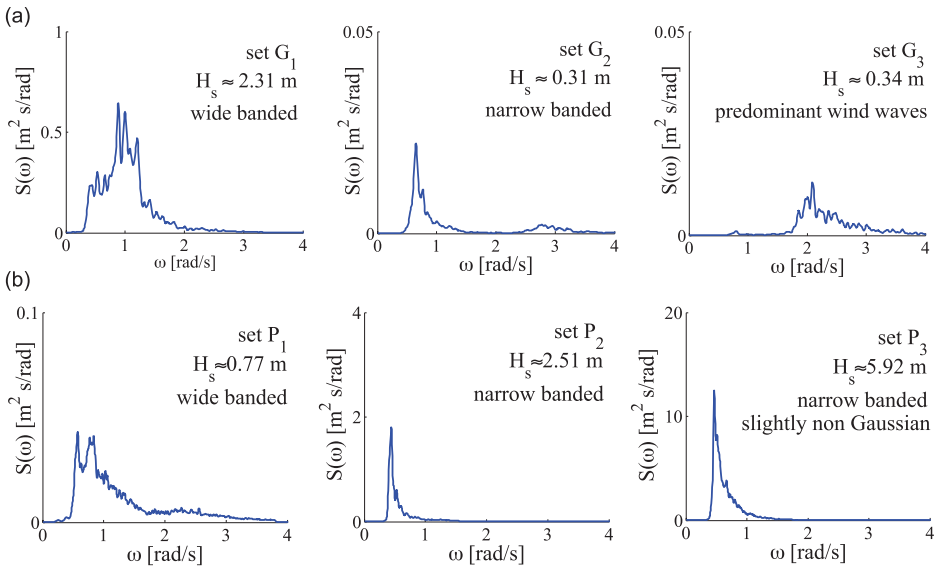

Figure 14. Wave spectra of sample data set for the two locations: (a) Galway bay, and (b) Pico island.

significant data sets at the two locations are shown in Figure 14. In this figure, most of the wave energy is concentrated at low frequencies, and it is therefore a reasonable assumption to low-pass filter the wave elevation and focus the prediction only on the low frequencies (Fusco and Ringwood 2010). The prediction accuracy of each forecasting model can be measured with the following goodness-of-fit index, for a forecasting horizon l:

$$F(l) = \left(1 - \frac{\sqrt{\sum_k \left[\eta(k+l) - \hat{\eta}(k+l|k)\right]^2}}{\sqrt{\sum_k \eta^2(k)}}\right) \cdot 100, \tag{34}$$

where $\eta(k+l)$ is the wave elevation and $\hat{\eta}(k+l|k)$ is its prediction based on the information up to instant k. A 100% value for $F(l)$ means that the wave elevation time series is perfectly predicted l steps into the future. In Figure 15, the prediction accuracy of different forecasting models is shown for two data sets, over a forecasting horizon of about 20 seconds. Initial observation of Figure 15 reveals that all the selected forecasting models perform better for the narrow-banded sea state P_2, as shown in Figure 15b, than for the broader-banded G_1, shown in Figure 15a.

In particular, the Harvey cyclical model and the sinusoidal extrapolation through the EKF are dramatically affected by the bandwidth of the wave signal and their $F(l)$ for the data set G_1 dies out relatively quickly, going below 0% after only 5 seconds. AR models offer much more accurate predictions further into the future than the cyclical models for all the sea states. In the case of P_2 (Fig. 15b), accuracy of $F(l) > 90\%$ is maintained for more than 20

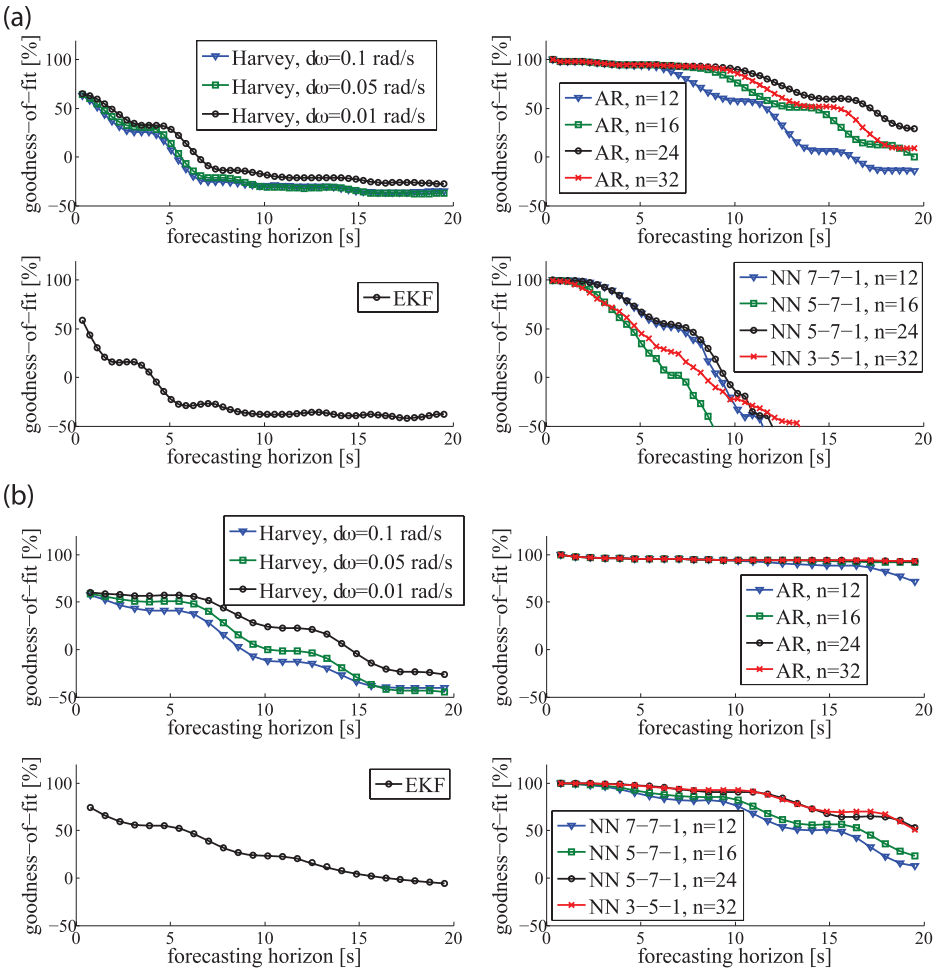

Figure 15. Goodness-of-fit $F(l)$ of different forecasting models on two data sets: (a) Galway bay set G_1, and (b) Pico set P_2.

seconds into the future, about 2 wave periods of a wave with period 10.47 s (corresponding to a peak frequency of 0.6 rad/s, as from Fig. 14). AR model performance is still affected by the bandwidth of the sea state, but relatively accurate predictions, $F(l) > 90\%$ for more than 10 seconds in the future, are still obtained for the set G_1, although higher order models, e.g., $n = 24$, 32, are required. For the neural networks, the results of some of the more promising configurations show a similar accuracy to AR models for the case of the narrow-banded sea state P_2, while the prediction diverges fairly quickly in the case of the data set G_1. The search of possible network configurations was not exhaustive, but was broad enough to conclude that artificial neural networks are not able to offer any significant

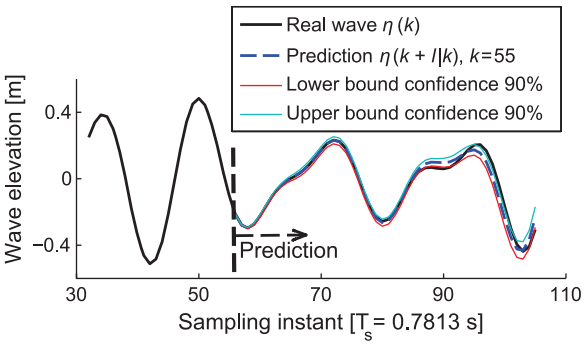

Figure 16. Confidence interval and predictions $\hat{\eta}(k+l|k)$, for $l = 1$ to $l = 50$, at a specific time instant k, calculated with an AR model of order $n = 24$ on the data set P_2, filtered with cut-off frequency $\omega_c = 0.7$ rad/s.

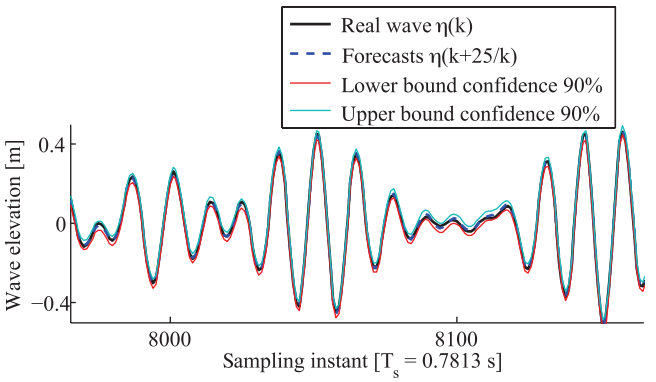

Figure 17. Confidence interval and 25-step-ahead predictions $\hat{\eta}(k+25|k)$, for some k, calculated with an AR model of order $n = 24$ on the data set P_2, filtered with cut-off frequency $\omega_c = 0.7$ rad/s.

improvement in the short-term prediction of the wave elevation over simple AR models to justify the higher complexity and the lack of any physical meaning. The detail of the prediction $\hat{\eta}(k+l|k)$ with an AR model on the data set P_2, at a specific instant $k = 55$ and for a forecasting horizon $l = 1$ to 50 samples (nearly 39 s), is shown in Figure 16, along with the 90% confidence interval, estimated according to the methodology described in (Fusco and Ringwood 2010). In Figure 17, the comparison between the real wave elevation and the 25-step-ahead prediction $\hat{\eta}(k+25|k)$ is shown, computed with an AR model of order $n = 24$, along with the corresponding 90% confidence interval.

c. Up-wave forecasting

An alternative approach to the time series forecasting is to reconstruct the wave elevation at the location of the WEC by means of the free surface elevation up-wave of the WEC, as

shown in Figure 13b. If the free surface elevation up-wave of the WEC propagates only in the direction towards the WEC, with a known propagation time, the incident wave elevation reaches the location of the WEC.

The propagation time can be inferred from considerations of wave propagation in a finite water depth. Assuming that there are no attenuation effects on the traveling wave, the wave elevation η propagates in the direction x, defined positive from the location of the up-wave sensor to the WEC, accordingly to the following expression (Korde 2013):

$$\eta(t,x) = A\cos(\omega t - k(\omega)x) = Re(Ae^{j(\omega t - k(\omega)x)}), \tag{35}$$

where $k(\omega)$ is the wave number, which is a function of the frequency ω and water depth h. The wave propagates with a phase velocity given by (Falnes 2002):

$$v_p = \frac{\omega}{k(\omega)}. \tag{36}$$

In shallow water with depth h, the waves can reach a maximum velocity $v_{max} = (gh)^{0.5}$, where g is the gravitation acceleration. If it is assumed that all the waves travel at the same phase velocity equal to the maximum velocity, then the free surface elevation up-wave of the WEC reaches the location of the WEC without any phase distortion. If d denotes the spatial distance between the point of measurement of the free surface elevation up-wave of the WEC and the location of the WEC, the propagation time t_{prop} of the wave is as follows (Korde 2013):

$$t_{prop} = \frac{d}{v_{\max}}. \tag{37}$$

If there are no nonlinearities or attenuation effects on the wave propagation, the use of the up-wave elevation measurement provides advance knowledge of the future wave elevation at the location of the WEC for a forecasting horizon equal to the propagation time. In Section 3ci, a forecasting model based only on the measurements of the free surface elevation up-wave of the WEC is presented, while in Section 3cii, a forecasting model based on a combination of the past history of the wave elevation and measurements of the free surface elevation up-wave of the WEC is derived.

i. Up-wave only models. In this section, a model for forecasting the wave elevation at the location of the WEC based only on the measurement of the free surface elevation up-wave of the WEC is presented. In particular, a Finite Impulse Response (FIR) model is designed which assumes that the wave elevation at the location of the WEC at time instant k is a linear combination of n_b past values of the free surface elevation up-wave of the WEC. The up-wave measurement is considered to be the input of the model and is denoted as u. The model considered is of the following form:

$$\eta(k) = \sum_{i=1}^{n_b} b_i u(k - i + 1 - n_k) + \xi(k), \tag{38}$$

where ξ is considered to be a white noise with zero mean and variance σ^2. The term n_k is the delay (in number of sample periods) that occurs before the output is affected by the input. If the data coming from the up-wave sensor are delayed by the propagation time then, at time instant k, the water level at the location of the WEC is influenced by the up-wave elevation at the same time instant. Therefore, the delay n_k is considered to be zero. The use of the FIR filter takes into account the dynamics between the up-wave elevation and the wave elevation at the location of the WEC, which is not considered in the calculation of the propagation time alone. Given a set of parameters b_i, from Eq. 38, the l-step ahead prediction is given as follows:

$$\hat{\eta}(k+l|k) = \sum_{i=1}^{n_b} b_i u(k+l-i+1). \tag{39}$$

The coefficients b_i of the FIR model are estimated through the minimization of the variance of the one-step ahead prediction error (Paparella et al. 2015):

$$J_{LS} = \sum_{k=1}^{N_1} \left[\eta(k+1) - \hat{\eta}(k+1|k)\right]^2, \tag{40}$$

which is a linear least squares (LS) problem.

ii. Combination up-wave/autoregressive models. In this section, a model for forecasting the wave elevation at the location of the WEC, based on a combination of its past history and measurements of the free surface elevation up-wave of the WEC, is presented. In particular, an autoregressive exogenous input (ARX) model is proposed which assumes that the wave elevation at the location of the WEC at time instant k is linearly dependent on a number n_a of its past values and on n_b values of up-wave measurements. Thus, the model considered is of the following form:

$$\eta(k) = \sum_{i=1}^{n_a} a_i \eta(k-i) + \sum_{i=1}^{n_b} b_i u(k-i+1) + \xi(k). \tag{41}$$

Given a set of parameters a_i and b_i, from Eq. 41, the l-step ahead prediction is given as follows:

$$\hat{\eta}(k+l|k) = \sum_{i=1}^{n_a} a_i \hat{\eta}(k+l-i|k) + \sum_{i=1}^{n_b} b_i u(k+l-i+1). \tag{42}$$

In Eq. 42, no prediction of the input is made until a prediction horizon, equal to the propagation time of the wave from the location of the sensor is reached. The limit of the prediction horizon, in time steps, is denoted as l_{max}, which is given as follows:

$$l_{\max} = \frac{t_{prop}}{t_{samp}} = \frac{d/v_p}{t_{samp}}, \tag{43}$$

where t_{samp} is the sampling time of the wave elevation at the location of the WEC and up-wave elevation. Therefore, the prediction of $\hat{\eta}$ can be made with an ARX model only until l_{max} steps, after which an AR only model is used to predict the water level at the location of the WEC. Thus, the complete prediction of the wave elevation using an ARX model is given as follows:

$$\hat{\eta}(k+l|k) = \begin{cases} \sum_{i=1}^{n_a} a_i \hat{\eta}(k+l-i|k) + \sum_{i=1}^{n_b} b_i u(k+l-i+1) & if\, l \le l_{\max} \\ \sum_{i=1}^{n_a} \alpha_i \hat{\eta}(k+l-i|k) & else \end{cases} . \quad (44)$$

The coefficients a_i, b_i of the ARX model and α_i of the AR model are estimated individually using the cost function given by Eq. 40.

d. Sample up-wave forecasting results

The forecasting models described in Section 3c were validated against real observations coming from the Pico WEC plant located on the Portuguese island of Pico in the Azores archipelago. In particular, two type of measurements were available: (i) measurements of the wave elevation inside the chamber of the Pico Oscillating Water Column (OWC) using a sonar mounted on the roof of the chamber, and (ii) measurements of the free surface elevation around 60 m in front of the Pico OWC. Two different types of up-wave sensors were deployed. During the first deployment period, the "Aquadopp" hydrostatic pressure sensor and ADCM (Acoustic Doppler Current Meter) unit was utilized, while during the second deployment period, an alternative "pneumatic sensor" which consists of small steel box, fixed on the sea floor with an open bottom, was deployed. The pneumatic sensor measures the change of the water level above from the variation of the air pressure inside the box.

The forecasting of the water level in the chamber given by the FIR and ARX models is compared with the forecasts given by the AR model over a certain range of prediction horizons. In order to compare the performance between the AR model and the FIR or ARX model, the Relative Goodness of Fit (RGOF) index is introduced:

$$\begin{aligned} RGOF_{FIR}(l) &= GOF_{FIR}(l) - GOF_{AR}(l) \\ RGOF_{ARX}(l) &= GOF_{ARX}(l) - GOF_{AR}(l) \end{aligned} . \quad (45)$$

The RGOF between an AR model of order $n_a = 30$ and a FIR model of order $n_b = 10$ is plotted against the forecasting horizon for the first and second deployment period in Figure 18a. As shown by Figure 18a, the AR model is able to provide more accurate predictions of wave elevation in the chamber for all forecasting horizons up to 7s, which is the propagation time of the incident wave from the location of the up-wave sensor to the chamber. For the first deployment period, in Figure 18b, the RGOF between an AR model

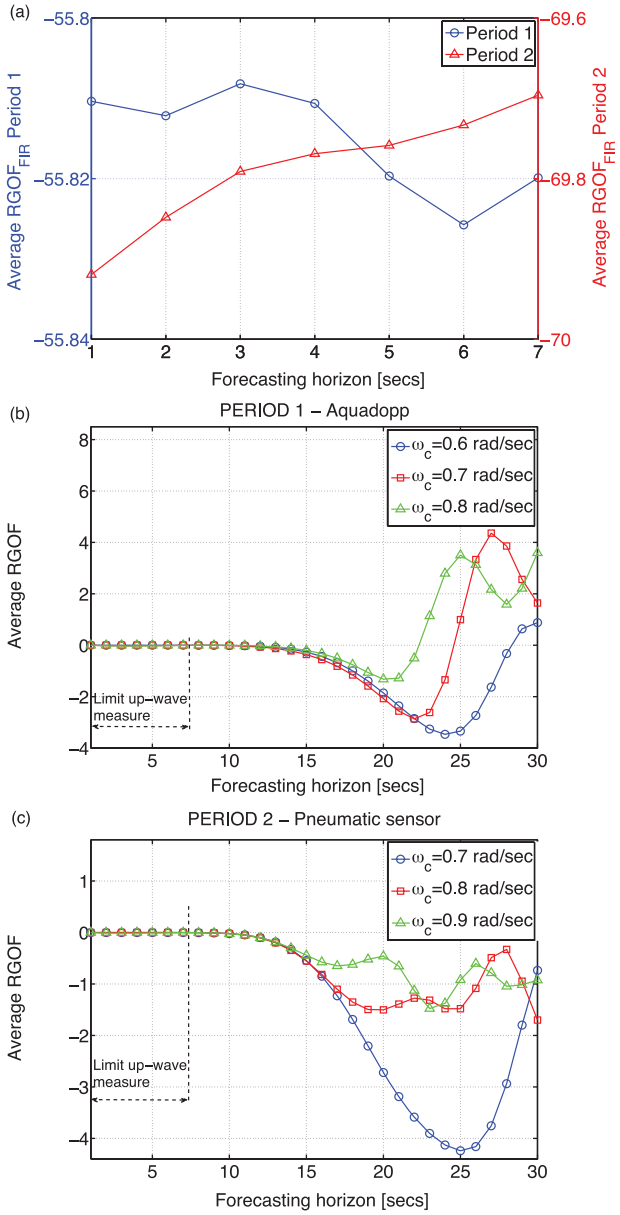

Figure 18. Relative Goodness of Fit (RGOF) between AR model ($n_a = 30$) and FIR model ($n_b = 10$) (a) between AR model ($n_a = 30$) and ARX model ($n_a = 30, n_b = 15$) for the first deployment period, (b) and between AR model ($n_a = 30$) and ARX model ($n_a = 30, n_b = 15$) for the second deployment period.

of order $n_a = 30$ and a ARX model of order $n_a = 30$ and $n_b = 15$ is plotted against the prediction horizon for different values of the cut-off frequency ω_c. As Figure 18b shows, the AR model performs better than the ARX model for prediction horizons that range from 10 seconds up to 22 or 27 seconds, depending on ω_c. The choice of the cut-off frequency ω_c depends on frequency components of the chamber wave elevation that need to be predicted.

Note that the improvement in the accuracy of the prediction of the chamber wave elevation for long horizons obtained with the ARX model has to be evaluated with respect to the prediction requirements in the control of the WEC. In fact, because of the noncausal transfer function involved in the realization of the real-time optimal control of the WEC, the future wave elevation may be needed until a time horizon up to 30 seconds (Fusco and Ringwood 2012). Regarding the second deployment period, in Figure 18c, the RGOF between an AR model of order $n_a = 30$ and an ARX model of order $n_a = 30$ and $n_b = 15$ is plotted against the prediction horizon for different values of the cut-off frequency ω_c. As Figure 18c shows, the ARX model provides less accurate predictions of the wave elevation inside the chamber than the AR model for every prediction horizon. A comparison between predicted and actual chamber wave elevations for a forecasting horizon of 30 seconds, for an ARX model of order $n_a = 30$ and $n_b = 15$, is made. The ARX model utilizes the free surface elevation up-wave of the WEC provided by the Aquadopp and pneumatic sensors, reported in Figures 19a and 19b, respectively.

5. Discussion and conclusion

Forecasting plays an important role in wave energy, on a variety of time and spatial scales. A number of processes in the wave energy design chain rely on forecasts and various causal inputs may be appropriate on the different time scales.

In the first instance, the viability of a wave energy project relies on a forecast (hindcast) of the likely wave energy that can be practically harvested in a particular location, with (historical) weather inputs providing the causal variables. This assessment is usually carried out over a long period, typically 1 to 10 years. For this application, the state-of-the-art procedure consists of downscaling the wave conditions from a global wind–wave model to account for the wave transformation processes that take place nearshore. Although several approaches are available to carry out a downscaling from a global wind–wave model, dynamic downscaling is the most widely used for wave resource characterization. Dynamic downscaling consists of using the outputs offered by a global wind–wave model to force a finer wave propagation model, which accounts for the nearshore wave transformation processes such as refraction, bottom friction, shoaling, diffraction, and breaking. Among wave propagation models, spectral wave models are the most popular choice for wave resource characterization, although their range of application does not extend to some applications such as very shallow waters and complex geometries. In addition, hindcasts for wave resource characterization are starting to present an advanced degree of standardization, with the aim of ensuring consistency and accuracy in wave resource assessment. In this context,

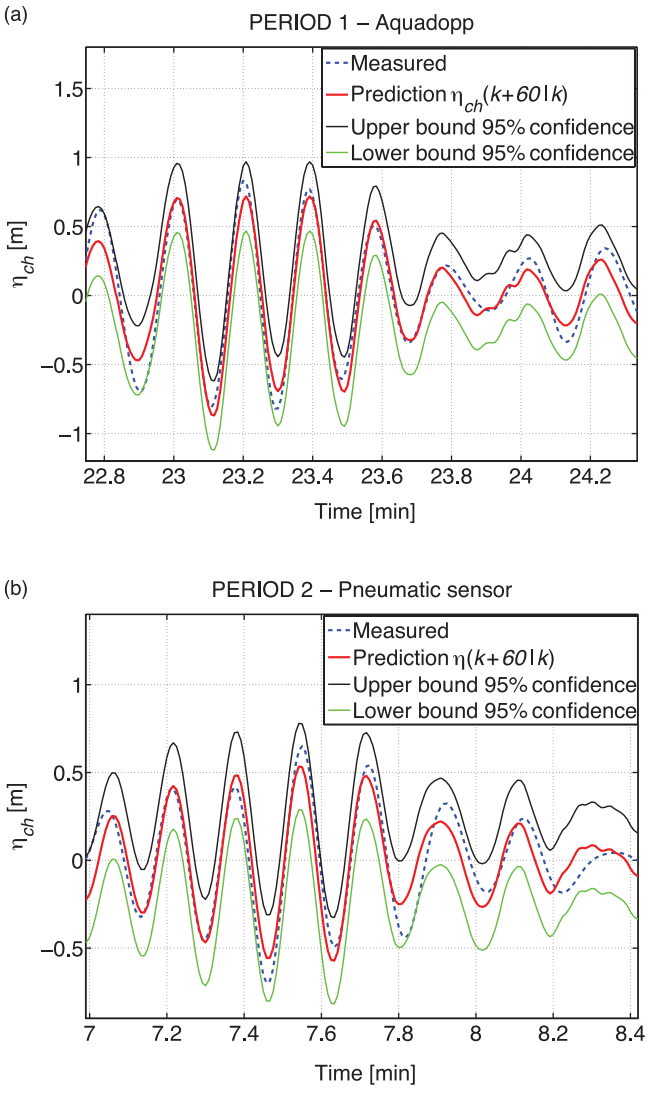

Figure 19. Comparison between measured chamber wave elevation and prediction $\eta_{ch}(k+60|k)$ computed with an ARX model of order $n_a = 30$ and $n_b = 15$ with data set of first (a) and second deployment period (b), filtered with a cut-off frequency of $\omega_c = 0.7$ rad/s.

the technical standard IEC-62600-201 stands out, which classifies the resource assessment studies into three different categories: reconnaissance, feasibility and design, offering for each class a wide set of recommendations regarding the procedure to follow in the fields of data collection, wave modeling, data analysis and the reporting of the results. Finally,

IEC-62600-201 has been tested against different wave climates, offering good results, and proving that the proposed methodology is robust and coherent.

In the medium-term horizon, the requirement is for wave energy production forecasts, in the context of market participation. The organization of power markets provides guidelines in terms of time resolution (in the order of half-hourly forecasts) and time horizons (from 2–3 days ahead to 1 h–30 minute ahead). Typical causal inputs at this time scale are also weather variables. Accurate power production forecasts will probably require a more detailed sea state representation than the classical power matrix device description, taking into account wave direction, spectral bandwidth, or other advanced descriptions of the spectral shape. Overall, there is still much space for investigation in medium-term wave power forecasting. It seems possible to successfully combine methods based on machine-learning and time-series, with forecasts based on physical models. However, current time-series and machine-learning models mainly predict scalar values, instead of a full directional spectrum. In the available literature, very basic sea state parameters are predicted this way, typically wave energy flux, or significant wave height and wave period. Adapting such tools to more advanced sea state descriptions is a valuable research direction. Finally, suitable WEC and sea state descriptions for wave energy forecasting still deserves more investigation.

For short-term wave forecasting, two different approaches are compared: time series and spatial approach. The time series approach uses no causal inputs and relies exclusively on an extrapolation of the historical time series. Regarding the time series approach, results on real wave elevation data from Galway Bay and Pico Island showed how a relatively simple AR model, which implicitly models the cyclical behavior of the waves, can offer a very accurate prediction of the low-frequency swell waves for up to two typical wave periods into the future. It was also shown that no real benefit can be expected in using nonlinear forecasting models, such as neural networks, unless highly nonlinear sea states are encountered, which are likely to beyond the power production operational region of WECs.

Regarding the spatial approach for short-term forecasting, a causal input is provided via wave sensors placed up-wave of the location of interest. Results on the real wave elevation data from the PICO plant show that there is little advantage in making an up-wave measurement, in terms of wave forecasting accuracy. This is useful information, allowing potential reductions in capital and maintenance costs. However, the generality of such a conclusion is uncertain. The Pico wave climate is reasonably stable, with a well-defined swell component. Furthermore, the forecasting problem for an OWC is straightforward, where the chamber water elevation is directly measurable, unlike the case of floating devices, where the free-surface elevation at the device location is impossible to measure, and the focus may need to change to excitation force.

Concerning the use of the wave prediction algorithms in real-time WEC control, the real-time filter implementation needs to be given further attention, since a zero-phase filter was assumed in the presented analysis. However, in general, the controller of a WEC is likely to require the prediction of an effect of the wave elevation on the device, e.g., the

wave excitation force, which is effectively a low-pass filtered version of the wave elevation, with the filtering provided by the device itself.

REFERENCES

Aparicio, N., I. MacGill, J. Rivier Abbad, and H. Beltran. 2012. Comparison of wind energy support policy and electricity market design in Europe, the United States, and Australia. IEEE Trans. Sustainable Energy, *3(4)*, 809–818. doi: 10.1109/TSTE.2012.2208771

Babarit, A. 2015. A database of capture width ratio of wave energy converters. Renewable Energy, *80*, 610–628. doi: 10.1016/j.renene.2015.02.049

Babarit, A., J. Hals, M. J. Muliawan, A. Kurniawan, T. Moan, and J. Krokstad, J. 2012. Numerical benchmarking study of a selection of wave energy converters. Renewable Energy, *41*, 44–63. doi: 10.1016/j.renene.2011.10.002

Battjes, J. A., and J. P. F. M. Janssen. 1978. Energy loss and set-up due to breaking of random waves. Coast. Eng. Proc. 1(16). Washington, D. C.: ASCE.

Belmont, M., J. Horwood, R. Thurley, and J. Baker. 2006. Filters for linear sea-wave prediction. Ocean Eng., *33(17–18)*, 2332–2351. doi: 10.1016/j.oceaneng.2005.11.011

Belmont, M. R., J. M. K. Horwood, R. W. F. Thurley, and J. Baker. 2007. Shallow angle waveprofiling lidar. Atmos. Ocean. Technol., *24(6)*, 1150–1156. doi: 10.1175/JTECH2032.1

Benoit, M. 2005. TOMAWAC software for finite element sea state modelling, release 5.5-User Manual. EDFLNHE, Chatou, France (distributed by HRWallingford).

Bretschneider, C. L. 1959. Wave variability and wave spectra for wind-generated gravity waves. Tech. Memo. No. 118. Beach Erosion Board, US Army Corps Of Eng., Washington, DC.

Browne, M., B. Castelle, D. Strauss, R. Tomlinson, M. Blumenstein, and C. C. Lane. 2007. Near-shore swell estimation from a global wind-wave model: Spectral process, linear, and artificial neural network models. Coast. Eng., *54(5)*, 445–460. doi: 10.1016/j.coastaleng.2006.11.007

Camus, P., F. J. Mendez, R. Medina, A. Tomas, and C. Izaguirre. 2013. High resolution downscaled ocean waves (DOW) reanalysis in coastal areas. Coast. Eng., *72*, 56–68. doi: 10.1016/j.coastaleng.2012.09.002

Carballo, R., M. Sánchez, V. Ramos, F. Taveira-Pinto, and G. Iglesias. 2014. A high resolution geospatial database for wave energy exploitation. Energy, *68*, 572–583. doi: 10.1016/j.energy.2014.02.093

Carballo, R., M. Sánchez, V. Ramos, and A. Castro. 2014. A tool for combined WEC-site selection throughout a coastal region: Rias Baixas, NW Spain. Appl. Energy, 135, 11–19. doi: 10.1016/j.apenergy.2014.08.068

Carballo, R., M. Sánchez, V. Ramos, J. A. Fraguela, and G. Iglesias. 2015. Intra-annual wave resource characterization for energy exploitation: A new decision-aid tool. Energy Conversion and Management, *93*, 1–8. doi: 10.1016/j.enconman.2014.12.068

Carballo, R., M. Sánchez, V. Ramos, J. A. Fraguela, and G. Iglesias. 2015. The intra-annual variability in the performance of wave energy converters: A comparative study in N Galicia (Spain). Energy, *82*, 138–146. doi: 10.1016/j.energy.2015.01.020

Castro, A., R. Carballo, G. Iglesias, and J. Rabuñal. 2014. Performance of artificial neural networks in nearshore wave power prediction. Appl. Soft Comput., *23*, 194–201. doi: 10.1016/j.asoc.2014.06.031

Dannenberg, J., K. Hessner, P. Naaijen, H. Van Den Boom, and K. Reichert. 2010. The on board wave and motion estimator OWME. In Proc. International Offshore and Polar Engineering Conference, pages 424–431.

De Andres, A. D., R. Guanche, J. A. Armesto, F. Del Jesus, C. Vidal, and I. J. Losada. 2013. Time domain model for a two-body heave converter: Model and applications. Ocean Eng., *72*, 116–123. doi: 10.1016/j.oceaneng.2013.06.019

De Andrés, A. D., R. Guanche, J. Weber, and R. Costello. 2015. Finding gaps on power production assessment on WECs: Wave definition analysis. Renewable Energy, *83*, 171–187. doi: 10.1016/j.renene.2015.04.026

ECMWF (European Centre for Medium-Range Weather Forecasts). 2017. Website (http://www.ecmwf.int/).

EPEX Spot (European Power Exchange). 2015. Press release 16 June 2015: EPEX SPOT and ECC to reduce intraday lead time on all markets.

Falcão, A. F. 2010. Wave energy utilization: A review of the technologies. Renew. Sustainable Energy Rev., *14*, 899–918. doi: 10.1016/j.rser.2009.11.003

Falnes, J. Ocean Waves and Oscillating Systems. Cambridge: Cambridge University Press.

Fernández, J., S. Salcedo-Sanz, P. Gutirrez, E. Alexandre, and C. Hervs-Martnez. 2015. Significant wave height and energy flux range forecast with machine learning classifiers. Eng. Appl. Artif. Intell., *43*, 44–53. doi: 10.1016/j.engappai.2015.03.012

Fischer, B., P. Kracht, and S. Perez-Becker. 2012. Online-algorithm using adaptive filters for short-term wave prediction and its implementation. In Proc. International Conference on Ocean Energy, 2012.

Folley, M., A. Babarit, B. Child, D. Forehand, L. O'Boyle, K. Silverthorne, et al. 2012. A review of numerical modelling of wave energy converter arrays. In ASME 2012 31st International Conference on Ocean, Offshore and Arctic Engineering; 535–545. doi: 10.1115/OMAE2012–83807

Frigaard, P., and M. Brorsen. 1995. A time-domain method for separating incident and reflected irregular waves. Coast. Eng., *24*, 205–215. doi: 10.1016/0378–3839(94)00035-V

Fusco, F. 2009. Forecasting requirements in the optimal control of wave energy converters. Tech. rep. EE/2009/2/JVR. NUI Maynooth, Ireland: Department of Electronic Engineering.

Fusco, F., and J. V. Ringwood. 2009. A study on short-term sea profile prediction for wave energy applications. In Proc. of the 8th European Wave and Tidal Energy Conf. (EWTEC), 2009, 756–765. doi: 10.1109/TSTE.2010.2047414

Fusco, F., and J. V. Ringwood. 2010. Short-term wave forecasting for real-time control of wave energy converters. IEEE Trans. Sustainable Energy, *1(2)*, 99–106. doi: 10.1109/TSTE.2010.2047414

Fusco, F., and J. V. Ringwood. 2012. A study on the prediction requirements in real-time control of wave energy converters. IEEE Trans Sustainable Energy, *3(1)*, 176–184. doi: 10.1109/TSTE.2011.2170226

Gallagher, S., R. Tiron, E. Whelan, E. Gleeson, F. Dias, and R. McGrath. 2016. The nearshore wind and wave energy potential of Ireland: a high resolution assessment of availability and accessibility. Renewable Energy, *88*, 494–516. doi: 10.1016/j.renene.2015.11.010

Group, T. W. 1988. The WAM model-a third generation ocean wave prediction model. J. Phys. Oceanogr., *18(12)*, 1775–1810. doi: 10.1175/1520-0485(1988)018<1775:TW MTGO>2.0.CO;2

Halliday, J. R., D. G. Dorrell, and A. R. Wood. 2011. An application of the Fast Fourier Transform to the short-term prediction of sea wave behaviour. IEEE Trans Renewable Energy, *36(6)*, 1685–1692. doi: 10.1016/j.renene.2010.11.035

Harvey, A. C. 1989. Forecasting, Structural Time Series Models and the Kalman Filter. Cambridge: Cambridge University Press, 1989.

Hasselmann, K. 1962. On the non-linear energy transfer in a gravity-wave spectrum. J. Fluid Mech, *12*, 481–500. doi: 10.1017/S0022112062000373

Hasselmann, S., and K. Hasselmann. 1985. Computations and parameterizations of the non-linear energy transfer in a gravity wave spectrum. Part I. A new method for efficient calculations of

the exact non-linear transfer integral. J. Phys. Oceanogr., *15*, 1369–1377. doi: 0.1175/1520-0485(1985)015<1369:CAPOTN>2.0.CO;2

Hasselmann, K., T. Barnett, E. Bouws, H. Carlson, D. Cartwright, K. Enke, et al. 1973. Measurements of wind-wave growth and swell decay during the Joint North Sea Wave Project (jonswap). Deut. Hydrograph. Inst. Tech. Rep., 1973.

Hasselmann, K., W. Sell, D. B. Ross, and P. Müller. 1976. A parametric wave prediction model. J. Phys. Oceanogr., *6(2)*, 200–228. doi: 10.1175/1520-0485(1976)006<0200:APWPM>2.0.CO;2

Hatalis, K., P. Pradhan, S. Kishore, R. Blum, and A. Lamadrid. 2014. Multistep forecasting of wave power using a nonlinear recurrent neural network. In PES General Meeting Conference Exposition, 2014 IEEE, 1–5. doi: 10.1109/PESGM.2014.6939370

Herman, A., R. Kaiser, and H. D. Niemeyer. 2009. Wind-wave variability in a shallow tidal sea—Spectral modelling combined with neural network methods. Coast. Eng., *56(7)*, 759–772. doi: 10.1016/j.coastaleng.2009.02.007

Hiles, C. E. 2010. On the use of computational models for wave climate assessment in support of the wave energy industry. Doctoral thesis, University of Victoria.

Hirth, L., and I. Ziegenhagen. 2015. Balancing power and variable renewables: Three links. Renewable Sustainable Energy Rev, *50*, 1035–1051. doi: 10.1016/j.rser.2015.04.180

Holthuijsen, L. H., N. Booij, R. C. Ris, I. J. G. Haagsma, A. T. M. M. Kieftenburg, and R. Padilla-Hernandes. 2000. SWAN User Manual. Delft: Department of Civil Engineering. Delft University of Technology.

IEC Technical Committee 114. 2014. IEC TS 62600-101: Technical Specification. Marine energy: wave, tidal and other water current converters: Part 101: wave energy resource assessment and characterization; edition 1.0. Draft technical specifications. Geneva: International Electrotechnical Commission (IEC). 8 p.

Iglesias, G., M. López, R. Carballo, A. Castro, J. A. Fraguela, and P. Frigaard. 2009. Wave energy potential in Galicia (NW Spain). Renewable Energy, *34(11)*, 2323–2333. doi: 10.1016/j.renene.2009.03.030

Jeon J., and J. Taylor. 2016. Short-term density forecasting of wave energy using ARMA-GARCH models and kernel density estimation. Int. J. Forecast., *32*, 991–1004. doi: 10.1016/j.ijforecast.2015.11.003

Kerbiriou, M. A., M. Prevosto, C. Maisondieu, A. Babarit, and A. Clément. 2007. Influence of sea-states description on wave energy production assessment. In Proceedings of the Seventh European Wave and Tidal Energy Conference, Porto, Portugal, 463–473. doi: 10.1115/OMAE2007-29254

Komen, G. J., Hasselmann, and K. Hasselmann. 1984. On the existence of a fully developed wind-sea spectrum. J. Phys. Oceanogr. *14(8)*, 1271–1285. doi: 10.1175/1520-0485(1984)014<1271:OTEOAF>2.0.CO;2

Korde, U. A. 2000. Control system applications in wave energy conversion. In Proc. OCEANS 2000 MTS/IEEE Conf. Exhibition, *3*, 1817–1824.

Korde, U. A. 2013. Up-wave surface elevation for smooth hydrodynamic control of wave energy conversion in irregular waves. In Proc. of the OCEANS'13 MTS/IEEE San Diego, 2013. doi: 10.23919/OCEANS.2013.6740965

Liberti, L., A. Carillo, and G. Sannino. 2013. Wave energy resource assessment in the Mediterranean, the Italian perspective. Renewable Energy, *50*, 938–949. doi: 10.1016/j.renene.2012.08.023

Lo, J. C. F., Z. L. Yang, and R. A. Pielke. 2008. Assessment of three dynamical climate downscaling methods using the Weather Research and Forecasting (WRF) model. J. Geophys. Res. Atmos., *113*, D09112. doi: 10.1029/2007JD009216

Mackay, E. 2016. A unified model for unimodal and bimodal ocean wave spectra. Int. J. Mar. Energy, *15*, 17–40. doi: 0.1016/j.ijome.2016.04.015

Maisondieu, C. 2015. WEC Survivability Threshold and Extractable Wave Power. In Proc. 11th Eur. Wave Tidal Energy Conf.

Miles, J. W. 1960. On the generation of surface waves by turbulent shear flows. J. Fluid Mech., *7(03)*, 469–478. doi: 10.1017/S0022112060000220

Mollison, D., and M. T. Pontes. 1992. Assessing the Portuguese wave-power resource. Energy, *17(3)*, 255–268. doi: 10.1016/0360-5442(92)90053-3

Monk, K., D. Conley, M. Lopes, and Q. Zou. 2013. Pneumatic power regulation by wave forecasting and real-time relief valve control for an OWC. In Proc. of the European Wave and Tidal Energy Conference Series, Aalborg, Denmark.

Nolan, G., J. V. Ringwood, and B. Holmes. 2007. Short term wave energy variability off the west coast of Ireland. European Wave and Tidal Energy Conference (EWTEC), 11–13 September 2007, Porto.

Norgaard, M., O. Ravn, N. Poulsen, and L. Hansen. 2000. Neural Networks for Modelling and Control of Dynamic Systems. New York: Springer. 246 p.

Ochi, M. K. 2005. Ocean Waves: the Stochastic Approach (Cambridge Ocean Technology Series 6) Cambridge: Cambridge University Press. 332 p.

Paparella, F., K. Monk, V. Winands, M. F. P. Lopes, D. Conley, and J. V. Ringwood. 2015. Up-wave and autoregressive methods for short-term wave forecasting for an oscillating water column. IEEE Trans. Sustainable Energy, *6(1)*, 171–178. doi: 10.1109/TSTE.2014.2360751

Pascal, R., G. Payne, C. M. Theobald, and I. Bryden. 2012. Parametric models for the performance of wave energy converters. Appl. Ocean Res., *38*, 112–124. doi: 10.1016/j.apor.2012.06.003

Phillips, O. M. 1957. On the generation of waves by turbulent wind. J. Fluid Mech., *2(05)*, 417–445. doi: 10.1017/S0022112057000233

Pinson, P., G. Reikard, and J.-R. Bidlot. 2012. Probabilistic forecasting of the wave energy flux. Appl. Energy, *93*, 364–370. doi: 10.1016/j.apenergy.2011.12.040

Price, A. A. E., and A. R. Wallace. 2007. Non-linear methods for next wave estimation. In Proc. 7th European Wave and Tidal Energy Conference, Porto, Portugal, 2007.

Quine, B., J. Uhlmann, and H. Durrant-Whyte. 1995. Implicit jacobians for linearised state estimation in nonlinear systems. In Proc. Am. Control Conf., 1995. doi: 10.1109/ACC.1995.529787

Ramos, V., and J. V. Ringwood. 2016. Exploring the utility and effectiveness of the IEC (International Electrotechnical Commission) wave energy resource assessment and characterisation standard: A case study. Energy, *107*, 668–682. doi: 10.1016/j.energy.2016.04.053

Reikard G., P. Pinson, and J.-R. Bidlot. 2011. Forecasting ocean wave energy: the ECMWF wave model and time series methods. Ocean Eng., *38(10)*, 1089–1099. doi: 10.1016/j.oceaneng.2011.04.009

Reikard G., B. Robertson, and J.-R. Bidlot. 2015. Combining wave energy with wind and solar: Short-term forecasting, Renewable Energy, *81*, 442–456. doi: 10.1016/j.renene.2015.03.032

Reikard G., B. Robertson, B. Buckham, J.-R. Bidlot, and C. Hiles 2015. Simulating and forecasting ocean wave energy in western Canada. Ocean Eng., *103*, 223–236. doi: 10.1016/j.oceaneng.2015.04.081

RES Legal Europe. 2014. European res-legal database on regulations on renewable energy generation in europe [Online]. Available: http://www.res-legal.eu/

Saulnier, J. B., A. Clément, A. F. de O. Falçao, T. Pontes, M. Prevosto, and P. Ricci. 2011. Wave groupiness and spectral bandwidth as relevant parameters for the performance assessment of wave energy converters. Ocean Eng., *38(1)*, 130–147. doi: 10.1016/j.oceaneng.2010.10.002

Schoen, M. P., J. Hals, and T. Moan. 2011. Wave prediction and robust control of heaving wave energy devices for irregular waves. IEEE Trans. Energy Convers., *26(2)*, 627–638. doi: 10.1109/TEC.2010.2101075

Shemdin, O., K. Hasselmann, S. V. Hsiao, and K. Herterich. 1978. Nonlinear and linear bottom interaction effects in shallow water. In Turbulent Fluxes Through the Sea Surface, Wave Dynamics, and Prediction. New York: Springer; 347–372. doi: 10.1007/978-1-4612-9806-9_23

Shook, D. S., C. Mohtadi, and S. L. Shah. 1991. Identification for long-range predictive control. IEEE Proc. D Control Theory and Applications, *138*, 75–84. doi: 10.1049/ip-d.1991.0010

SWAMP Group. 1985. Ocean Wave Modeling. New York: Plenum Press, 256 pp.

SWAN Team. 2007. SWAN User Manual. Delft, the Netherlands: Delft University of Technology.

Tedd, J., and P. Frigaard. 2007. Short term wave forecasting, using digital filters, for improved control of wave energy converters. ISOPE: International Offshore and Polar Engineering Proceedings, *2007*, 388–394. Mountain View CA: International Society of Offshore and Polar Engineers (ISOPE).

Tolman, H. L. 1991. A third-generation model for wind waves on slowly varying, unsteady, and inhomogeneous depths and currents. J. Phys. Oceanogr., *21*,782–797. doi: 10.1175/1520-0485(1991)021<0782:ATGMFW>2.0.CO;2

van Mierlo, F. A. J. M. 2014. Numerical modelling of wave penetration in ports. MS.c. thesis, T.U. Delft, Delft University of Technology.

Veigas, M., V. Ramos, V., and G. Iglesias, G. 2014. A wave farm for an island: Detailed effects on the nearshore wave climate. Energy, *69*, 801–812. doi: 10.1016/j.energy.2014.03.076

Vicinanza, D., L. Cappietti, V. Ferrante, and P. Contestabile. 2011. Estimation of the wave energy in the Italian offshore. J. Coast. Res., *64*, 613–617.

Wang, Q. C. Zhang, Y. Ding, G. Xydis, J. Wang, and J. Østergaard. 2015. Review of real-time electricity markets for integrating distributed energy resources and demand response. Appl. Energy, *138*, 695–706. doi: 10.1016/j.apenergy.2014.10.048

Waters, R., J. Engström, J. Isberg, and M. Leijon. 2009. Wave climate off the Swedish west coast. Renewable Energy, *34(6)*, 1600–1606. doi: 10.1016/j.renene.2008.11.016

Wilamowski, B. M. W., S. Iplikci, O. Kaynak, and M. O. Efe. 2001. An algorithm for fast convergence in training neural networks. Neural Networks, 2001, 1778–1782. doi: 10.1109/IJCNN.2001.938431

World Meteorological Organization (WMO). 1998. Instruments and Observing Methods. Guide to Wave Analysis and Forecasting (2nd ed.). WMO Rep. No. 72. Geneva: Secretariat of the World Meteorological Organization.

Wu, Y. K., and J. S. Hong. 2007. A literature review of wind forecasting technology in the world. Power Tech, 2007 IEEE Lausanne, *2007*, 504–509. IEEE. doi: 10.1109/PCT.2007.4538368

Received: *1 October 2015*; revised: *16 September 2016*.

Editor's note: Contributions to *The Sea: The Science of Ocean Prediction* are being published separately in special issues of *Journal of Marine Research* and will be made available in a forthcoming supplement as Volume 17 of the series.